

Preliminary Evidence of Transport-Limited Chemical Weathering and Element Immobility in the Ganges Tidal Delta Plain of Bangladesh

John C. Ayers^{1,1}, Brooke L. Patton^{1,1}, and Matthew J. Dietrich^{1,1}

¹Vanderbilt University

November 30, 2022

Abstract

Previous studies have documented a weathering-limited regime in the upper reaches of the Ganges River Basin. Chemical weathering and element mobility at six sites in the lower reaches of the Ganges in the tidal floodplain of Southwest Bangladesh were investigated by comparing compositions of rice paddy soils, precursor tidal channel sediments, surface waters, and extract solutions, which represent the soluble fraction of solids. Little spatial variation in water and solid compositions is observed in each season, indicating similar processes are acting to transport elements across this region. Roughly one to several decades after deposition, rice paddy soils are not significantly different in mineralogy or composition from precursor tidal channel sediments, and both are similar to the composition of average upper continental crust. There is no detectable change in composition of tidal channel water between upstream and downstream sites. Rice paddy and tidal channel waters are saturated in the dominant minerals present in the silt-sized soils and sediments, including quartz and clay minerals. Together, these observations indicate the dominance of weathered material and weak chemical weathering in the tidal floodplain, consistent with a transport-limited regime. Multiple lines of evidence indicate a lack of exchange equilibrium between surface waters and coexisting solids, which may be a common feature in tidal river deltas where transport-limited regimes likely dominate.

Hosted file

essoar.10502497.2.docx available at <https://authorea.com/users/533161/articles/607673-preliminary-evidence-of-transport-limited-chemical-weathering-and-element-immobility-in-the-ganges-tidal-delta-plain-of-bangladesh>

Preliminary Evidence of Transport-Limited Chemical Weathering and Element Immobility in the Ganges Tidal Delta Plain of Bangladesh

J. C. Ayers¹, B. Patton¹, and M. Dietrich¹

¹ Department of Earth and Environmental Sciences, Vanderbilt University. VU Station B, #351805, 2301
Vanderbilt Place, Nashville, Tennessee 37235-1805, U. S. A.

Corresponding author: John C. Ayers (john.c.ayers@vanderbilt.edu)

Key Points:

- In the Ganges tidal delta plain in Bangladesh chemical weathering rates are low and transport-limited.
- Tidal channel sediments and rice paddy soils are similar in chemical composition to average upper continental crust.
- Relative to coexisting solids, surface waters are depleted in immobile elements but are not in exchange equilibrium.

Abstract

Previous studies have documented a weathering-limited regime in the upper reaches of the Ganges River Basin. Chemical weathering and element mobility at six sites in the lower reaches of the Ganges in the tidal floodplain of Southwest Bangladesh were investigated by comparing compositions of rice paddy soils, precursor tidal channel sediments, surface waters, and extract solutions, which represent the soluble fraction of solids. Little spatial variation in water and solid compositions is observed in each season, indicating similar processes are acting to transport elements across this region. Roughly one to several decades after deposition, rice paddy soils are not significantly different in mineralogy or composition from precursor tidal channel sediments, and both are similar to the composition of average upper continental crust. There is no detectable change in composition of tidal channel water between upstream and downstream sites. Rice paddy and tidal channel waters are saturated in the dominant minerals present in the silt-sized soils and sediments, including quartz and clay minerals. Together, these observations indicate the dominance of weathered material and weak chemical weathering in the tidal floodplain, consistent with a transport-limited regime. Multiple lines of evidence indicate a lack of exchange equilibrium between surface waters and coexisting solids, which may be a common feature in tidal river deltas where transport-limited regimes likely dominate.

Plain Language Summary

Previous studies of the upper reaches of the Ganges River near the Himalaya have shown that an abundant supply of easily weathered minerals produced by erosion results in rapid chemical weathering. We measured the chemical compositions of water from rivers and rice paddies, and of associated river sediments and the soils that form from them, in the lower reaches of the Ganges River tidal delta plain in SW Bangladesh. We found that soils were similar in composition to river sediments, and that river water compositions were constant across our study area. These observations suggest that little material is transferred from solids to water over the course of roughly one decade. Evidence suggests that this is either because the soluble minerals were

manuscript submitted to *Geochemistry, Geophysics, Geosystems (G3)*
dissolved in the upper reaches and are not present in sediment in the lower reaches, or the water has dissolved as much of the minerals as possible.

1 Introduction

Roughly 1×10^9 tonnes of sediment per year are eroded from the Himalaya and transported through the Ganges-Brahmaputra-Meghna (GBM) delta (Milliman & Farnsworth, 2013). Chemical weathering of silicates in these sediments and subsequent precipitation of carbonates is hypothesized to have caused drawdown of atmospheric CO₂ and global cooling in the Cenozoic (Raymo & Ruddiman, 1992) and to have increased seawater ⁸⁷Sr/⁸⁶Sr over the last 40 Myr (Edmond, 1992). Recent studies have found that chemical weathering of sediments occurs not just in the Himalayan source and in rivers, but also in the upper delta floodplain (Bickle et al., 2018; Lupker et al., 2012). This region is a weathering-limited regime because the rate of physical erosion is greater than the rate of chemical weathering (Stallard & Edmond, 1983; White & Buss, 2014). Because the rate of sediment supply is high due to rapid exhumation and erosion in the Himalayan source, the rate of chemical weathering is high. Readily weathered minerals such as plagioclase persist and weather in the floodplain, and weathering causes measurable changes in the composition of suspended sediments (Lupker et al., 2012) and dissolved loads (Bickle et al., 2018) in the Ganges upstream of Harding Bridge in Bangladesh. In a transport-limited regime in flat terrains, the amount of fresh rock available to weathering is limited by the rate of transport (Stallard & Edmond, 1983). Chemical weathering rates should decrease downstream as the rate of supply of unweathered primary minerals slows until a transport-limited regime is reached in the lower Ganges tidal plain, as hypothesized by Bickle et al. (2018), but this has not been tested.

In this study the compositions of rice paddy soils with approximately known ages, and tidal channel sediments are compared to qualitatively assess the effects of chemical weathering in the Ganges tidal delta plain in Southwest Bangladesh, ~340 km downstream from Harding Bridge (Fig. 1). A small number of upstream and downstream tidal channel water samples are compared to see if floodplain weathering in the tidal plain contributes dissolved solutes. We also evaluated the mobilities of major and trace elements by measuring

manuscript submitted to *Geochemistry, Geophysics, Geosystems (G3)*
apparent distribution coefficients of 22 elements between solids and coexisting water or deionized water
extracts, and investigated spatial and seasonal influences.

1.1 Setting

Bangladesh has a tropical, seasonal climate, with 80% of rainfall occurring during the monsoon from June to September (N. T. Chowdhury, 2010). The coastal region of Southwest Bangladesh consists of polders, islands surrounded by and separated from tidal channels by embankments. The tidal channels experience large seasonal changes in water salinity from ~0 ppt in the wet season to an average of ~15 ppt in the dry season for our study area (Ayers et al., 2017). Salinity can also vary on a diurnal and biweekly cycle, with higher salinity at spring high tide due to the increased proportion of seawater from the Bay of Bengal (Ayers et al., 2017). Tidal channels are the primary source of irrigation water in this region, because the local groundwaters are largely saline (Benneyworth et al., 2016; Naus et al., 2019). In the wet season when tidal channels contain fresh water, farmers grow rice in paddies. In the dry season when tidal channel water is saline, some farmers switch to brine shrimp aquaculture, while others with access to fresh groundwater use it to irrigate rice paddies (Barmon et al., 2010).

The Ganges catchment has an area of $\sim 10^6$ km², and starts in the steep Himalayan source terrain. As the main stem river collects water from tributaries and flows from the Himalayan source to the Bay of Bengal, it passes through sandy, steep alluvial fans, the upper delta floodplain, and then the relatively flat tidal delta plain. Annual discharge is between 380 and 590 km³/y, and suspended load is between 316 and 729 x 10⁶ t/y (Garzanti et al., 2019).

The region of study is in the Ganges tidal delta plain in the western portion of the lower GBM delta (Fig. 1). Besides intensively cultivated polders, it includes the Sundarbans National Forest, the world's largest littoral mangrove forest (Hale et al., 2019). The study area is in an abandoned lobe of the delta, largely cut off from the main Ganges river stem and dominated by tidal deposits. In this Ganges tidal delta plain, the deposits are considered estuarine because there is significant landward transportation of sediment sourced from the mouth of

manuscript submitted to *Geochemistry, Geophysics, Geosystems (G3)*
the GBM river by way of the inner shelf (M. Allison & Kepple, 2001; Rogers et al., 2013). More recent work has shown that the subareal delta has mineralogy more similar to Ganges sediments, while Bengal shelf sediments have a greater Brahmaputra sediment signature, suggesting that landward tidal transport of sediments derived from the shelf may not be important (Garzanti et al., 2019). Tidal deltaic deposits define the surficial geology, with upper silt and clay thicknesses from just a few meters up to 20 to 30 meters (MA Allison et al., 2003; Ayers et al., 2016). No previous studies have investigated how the composition of these deposits change after deposition.

1.2 Factors influencing compositions of solids

The mineralogy and chemical composition of sediments deposited by rivers depends on source characteristics; grain size sorting resulting from hydraulic effects, such as selective entrainment and settling; and chemical weathering during transport (Garzanti et al., 2010, 2011). Ganges River sediments are mainly sourced from the High Himalayan Crystalline series, with secondary contributions from the Lesser Himalaya and Indian craton (Goodbred et al., 2014). In the Ganges River basin the chemical composition of sediments primarily depends on mineral sorting and, therefore, grain size and density, and secondarily on depletion of mobile elements by chemical weathering in the floodplain (Lupker et al., 2012). The study area is in the distal portion of the Ganges basin, where sediments are often reworked and well-mixed (Rogers et al., 2013). Analysis of sediment in the $< 20 \mu\text{m}$ size fraction along the full 1700 km length of the Ganges River showed little variation in element concentrations and no evidence of heavy metal pollution (Singh et al., 2003). A previous study of Sundarbans sediment showed that concentrations of most metals were similar to or lower than in average upper continental crust (UCC), indicating little or no pollution (Islam et al., 2017). Sediments on polders near the Sundarbans should be similarly unaffected, since there is no industrial activity in this predominantly agricultural region. In the Sundarbans, where sediment deposition is unaffected by human activity, the median grain size is $31 \mu\text{m}$ (medium silt) near the Sutarkhali tidal river, decreases inland, and does not change seasonally (Hale et al., 2019).

Tidal islands in SW Bangladesh were converted to polders in the 1960s by building embankments. This reduced the frequency of flooding and, therefore, the sediment deposition rate on the polders (Auerbach et al., 2015). Today, tidal channel sediments are deposited on polders only when embankments are breached deliberately for tidal river management (Gain et al., 2017), when sluice gates are temporarily opened, or by storm surges that breach the embankments. For example, in 2009 Cyclone Aila caused long-term tidal flooding on Polder 32 due to embankment failures, which is a key area of this study (Fig. 1). This caused an elevated mean sediment deposition rate of 17.8 cm/yr determined by logging sediment cores (Auerbach et al., 2015). In contrast, the natural background rate of sedimentation at Polder 32 indicates average Holocene deposition of ~0.6-0.8 cm/y based on ^{14}C ages (Ayers et al., 2016). This compares well to modern sediment trap measurements in the Sundarbans that yield average annual sediment deposition (vertical accretion) rates of ~1 cm/y (Rogers et al., 2013), but with seasonality, from ~0.9 cm/y in the dry season to 1.2 cm/y in the wet season for island interiors (Bomer et al., 2020). We use these deposition rates to estimate mean elapsed time since sediment deposition, and thus the amount of time rice paddy soils were exposed to chemical weathering.

The silt-sized sediments deposited on polders are transported in tidal channels as suspended sediment. Studies of Ganges River sediments show that suspended sediment mineralogy and composition in the Ganges depends primarily on grain size, which varies from fine to medium silt at the surface to coarse silt and fine sand above the channel bed (Garzanti et al., 2011). Common minerals include quartz, feldspar, mica, calcite, dolomite, and epidote-amphibole-garnet suites, with slow-settling phyllosilicates and the elements they host concentrated near the surface (Garzanti et al., 2011). When first deposited on polders, sediments are likely to inherit the texture, mineralogy, and composition of shallow suspended sediments as the tidal river overtops or breaches the embankment.

The main pedogenic processes that convert sediment to soil in low-lying regions such as SW Bangladesh are (i) homogenization through bioturbation, (ii) mechanical weathering by plant roots, (iii) oxidation-reduction processes of Fe and Mn, (iv) accumulation of organic matter, (v) conversion of primary to secondary minerals such as clays through acid hydrolysis, and (vi) base leaching from calcareous top soils

(Hugh Brammer, 2016; Chen et al., 2011). Oxidation of iron under aerobic conditions produces rust colored soils, whereas the reduction of iron when soil is saturated and anaerobic produces grey colored soils (Horneman et al., 2004). Rice paddy soils in the tidal delta plain are often exposed to aerobic conditions in the dry season and anaerobic conditions in the wet season due to waterlogging, resulting in the formation of both rust and grey colored patches in soils (Brammer, 2016). In 2012 on Polder 32 we observed laminations in pits excavated for ponds. These laminations formed by daily tidal inundation following the breach of embankments during Cyclone Aila in 2009 (Auerbach et al., 2015). Soil horizon development was not observed, indicating the soils were entisols (Fry, 2015) and that sediments remained relatively unaltered at least three years after deposition.

1.3 Chemical Weathering in the Ganges Basin

Weathering-limited denudation regimes occur in steep terrains where the removal of weathered material is more rapid than chemical weathering, partially weathered solid material is eroded, and only a thin soil develops (Stallard and Edmond, 1983). Transport-limited denudation regimes occur in flat terrains in which solid materials have a long time to react with water, and thick soils develop (Maher, 2010). In transport-limited regimes the rate of chemical weathering is limited by the rate of erosion/supply of fresh sediment, so weathering rates may be low even in tropical climates (West et al., 2005). Sediments in transport-limited catchments are rich in stable, cation-depleted minerals such as quartz, kaolinite, and hydrous ferric oxides (HFOs) (Stallard & Edmond, 1983). Chemical weathering is faster in a weathering-limited regime than in a transport-limited regime because the most reactive phases are available for weathering, and the headwaters have lower solute contents and saturation indices.

In the upper reaches of the Ganges Basin, transported sediments are incompletely weathered, and floodplain weathering contributes a substantial fraction of weathering fluxes (Bickle et al., 2018; Lupker et al., 2012). However, no previous studies have explored chemical weathering in the lower reaches of the Ganges Basin. We hypothesize that in the Ganges tidal floodplain, chemical weathering should be transport-limited and lower than upstream in the alluvial fan and delta floodplain due to an inadequate supply of unweathered

sediment. In the tidal floodplain the rate of chemical weathering may also be low due to high solute contents that make surface waters saturated in available minerals; the presence of detrital carbonate minerals in the commonly deposited calcareous alluvium, which buffer pH to alkaline values and limit the weathering of minerals by acid hydrolysis (Brammer, 2016); and by the presence of swelling clays such as smectites produced by chemical weathering that make surface deposits impermeable (Benson et al., 1994). On the other hand, chemical weathering should be rapid in the ambient tropical climate, and may be accelerated by tilling and fertilization of rice paddy soil (Gandois et al., 2011).

1.4 Sampling Sites

Six sites chosen for this study spanned a wide range of surface water salinity and irrigation practices (Patton, 2018). Five sites were primarily used for agriculture, while one located in the Sundarbans mangrove forest represents natural background (Table 1, Fig. 1). Detailed site maps are given in Figures S1-S4. The dominant soil type in this region is noncalcareous grey floodplain soil that is seasonally flooded and can develop deeper than 25 cm in noncalcareous alluvium (H Brammer, 2012). The soils on Polder 32 were deposited immediately after Cyclone Aila, seven years before sample collection. For sites outside Polder 32 that were not inundated by Aila, the average time since deposition of the top 15 cm is less certain. Given that the long-term average regional sedimentation rate on polders is ~ 1 cm/y (Rogers et al., 2013), the average age of the top 15 cm would be ~ 7.5 years, not much different from the age of sampled deposits on Polder 32. However, it's unclear how much the relatively recent conversion of tidal islands to polders by addition of artificial levees, and their periodic breaching, has affected the average deposition rate, adding uncertainty to the age estimate.

2 Materials and Methods

2.1 Sample Collection and Field Measurements

Solid and water samples were collected at six sites (Fig. 1) in the dry season in May 2016 and wet season in November 2016 in order to describe spatial and temporal variations. Multiple samples from different locations were collected at each site (see site maps from Figures S1-S4). Solid and water samples were collected from the same locations in rice paddies, tidal channels, and the Sundarbans. Rice paddy soil samples were collected from the uppermost 15 cm to represent the cultivated topsoil, or ‘root zone’ (Barmon et al., 2010). Rice paddy samples were collected from inundated paddies, while sample type “Dry Rice Paddy” was collected from a part of the paddy without standing water, usually in the dry season. Comparison of the chemical compositions of our collected samples showed that dry rice paddy samples were not significantly different in composition from rice paddy samples with standing water, so these soil types are grouped together. Tidal channel sediment samples were collected from as close to the middle of the channel as possible, usually from irrigation canals connected to tidal channels because the latter were too deep and wide for sampling. Roughly one kg of solid was collected for each sample.

A Decagon GS3 probe was used to measure soil moisture, temperature, and electrical conductivity in-situ in November 2016, and a Hach HydroLab DS5 Sonde was used to measure water temperature, pH, redox potential Eh, and specific conductivity (SpC) in-situ. Sample locations were recorded using a Trimble GeoXT 6000, with a horizontal accuracy of 50 cm.

Tidal channel water samples were usually collected from the middle of the channel and water column in irrigation canals, but water in the canals was sourced from shallow levels of the tidal channels. Rice paddy water samples were also collected from the middle of the water column. Water samples were collected by rinsing a one L bottle, filling it, and immersing a Hydrolab DS5 Sonde for field measurements. Rainwater samples were collected in clean glass dishes set out just before a rain event. Next, a syringe was used to withdraw 30 mL from either a one L bottle after field measurements, or a clean glass dish. Water was then

manuscript submitted to *Geochemistry, Geophysics, Geosystems (G3)*
filtered at 0.45 μm into a polyethylene sample bottle. One drop of concentrated nitric acid (HNO_3) was added to the bottle before Inductively Coupled Plasma (ICP) analysis. Another 60 mL was filtered and placed in a sample bottle without acid for Ion Chromatography (IC) and Total Organic Carbon (TOC) analysis.

2.2 Sample Preparation

Solid samples were air dried, sieved with a No. 10 sieve, and homogenized by powdering in a mortar and pestle. Two to three grams were used to measure loss on ignition (LOI) at 105°C for H_2O - (adsorbed water) content and 1000°C for H_2O + (structural water) content in an alumina crucible (Pansu & Gautheyrou, 2007). A second split for extract preparation was dried at 110°C. Ten grams of solid was weighed and added to 50 mL of deionized water to form a slurry. The slurry was stirred for 15 minutes, then measured for pH using an Accumet pH meter and SpC using a HANNA Portable Solution Conductivity Measurement Meter (Tan, 2005). The saturated slurries were then filtered using a vacuum pump, coarse porosity/fast flow filter paper, and a Büchner flask and funnel. The extracts were filtered for a second time through a 0.45 μm syringe filter. Fifteen mL was placed in a conical vial, and 300 μL of concentrated nitric acid was added to make a 1% HNO_3 acid solution for ICP analysis. Another 30 mL was saved unacidified for IC and TOC analysis. All water and extract samples were refrigerated until analysed.

After LOI measurement, lithium metaborate (LiBO_2) fusion was completed using the same solid samples to measure their bulk composition. One hundred mg of solid sample and 600 mg LiBO_2 powder were weighed using an analytical balance and then mixed with an agate mortar and pestle under acetone. The mixture was air dried and transferred using weighing paper to a new graphite crucible. The crucible was then placed in a preheated oven for 10 minutes at 1100°C. The molten bead that had formed was poured into 50 mL of hot 1 molar (M) nitric acid (HNO_3) and stirred until the solid material was no longer visible (a minimum of 5 minutes). The cooled sample was transferred to a 50 mL centrifuge tube and brought to a volume of 50 mL by adding 1 M HNO_3 .

2.3 Laboratory Analysis

Samples of water, extracts, and dissolved solids were analyzed using methods described in Ayers et al. (2016), who also list method detection limits. Anions were measured in water and extract samples using ASTM Method D-4327-03 on a Metrohm 881 Compact IC Pro. Dissolved inorganic carbon (DIC) and dissolved organic carbon (DOC) were measured in water and extract samples using ASTM Method D-7573-09 on a Shimadzu model TOC-V CPH/CPN. Major cations were analyzed for using EPA Method 6010B on a Varian ICP Model 14720-ES ICP-OES. Trace metals were measured using a Perkin Elmer model ELAN DRC II ICP in both standard and dynamic reaction chamber (DRC) modes.

Select solid samples were analyzed for particle size using a Malvern Mastersizer 2000. A homogeneous subset of each solid sample analyzed was placed in a 1 L beaker of deionized water after running deionized water through the instrument to establish background concentrations. Sample were then deflocculated while suspended in deionized water via sonication before analysis. Samples were analyzed for the grain size range of 0.563 μm to 1.27 mm.

Minerals in select solid samples were identified using powder x-ray diffraction at Vanderbilt University. Dried, homogenized powder samples were dry cast on 20 x 20 mm square sample glass holders with a 0.2 mm indent and analyzed with a Rigaku SmartLab powder X-ray diffractometer with a Cu source of X-rays with a $\text{K}\alpha$ wavelength of 0.154 nm at 40 kV and 44 mA. The detector was a D/teX Ultra 250 1D silicon strip detector. PDXL software identified the mineral phases associated with the intensity peaks.

Clay mineralogy was determined in select samples using methods described in Pickering et al. (2017). Non-oriented powder scans were obtained on a Scintag X1 θ/θ automated powder XRD with a Cu target, a Peltier-cooled solid-state detector, and a plastic sample holder. Each sample underwent a set of three analyses: (1) the air-dried sample was analysed for smectite + illite and kaolinite + chlorite clay minerals; (2) the sample was glycolated for 12 h at 60°C to expand the smectite layers for analysis; (3) the sample was heated at 550°C to break down illite and analyse chlorite. Estimates of the relative abundance of clay minerals were determined

manuscript submitted to *Geochemistry, Geophysics, Geosystems (G3)*
for illite, smectite, chlorite, and kaolinite by measuring the mineral peak area and dividing by the mineral intensity factor, after Biscaye (1965).

Saturation index calculations were performed using the Spec8 program in Geochemists Workbench v.8 with the default thermo.dat database (Bethke, 2007). Data analysis was performed in R (R Core Team, 2019). Spatial analysis was conducted using ArcGIS Pro.

2.4 Quality Assurance/Quality Control

Deionized water was used for water sample blanks to test for water contamination in the field, and duplicates of select samples were collected in order to quantify precision. Water samples were kept refrigerated and were analyzed less than one month after collection. Our previous work has shown that, except for nitrate ions, measured concentrations do not change for at least one month after sample collection (Ayers et al., 2017). Charge imbalance errors for water samples averaged 4.1%, with the maximum being 21%. Measured concentrations for species reported here were well above the method detection limit (given in Ayers et al., 2016) for most elements, and sample concentrations were always significantly higher than blank concentrations. For duplicate water samples, the average percent difference in measured major element concentrations was 1.6%, indicating good precision. For water samples, total dissolved solids calculated from chemical analyses showed excellent correlation with values measured using the Hydrolab (adj. $r^2 = 0.994$, $n = 52$). For extract solutions a comparison of major elements in duplicate sample analyses shows an average percent difference of 8.7%. Charge imbalance on extract analyses averaged 0.68%, with a maximum of 9.0%.

Bulk solid procedures were also performed using 99.9% SiO_2 to test for contamination. Except for SiO_2 , oxide concentrations in these bulk solid blanks were on average 95% lower than concentrations measured in samples. USGS reference powders AGV-2 and GSP-2 were run as samples through the solid preparation procedures to test for accuracy, and duplicates were completed to quantify precision. Normalized AGV-2 major oxide concentrations were on average 12.6% different than the USGS reference, while GSP-2 oxides resulted in

manuscript submitted to *Geochemistry, Geophysics, Geosystems (G3)*
an average difference of 5.8%. Most trace element concentrations were within 20%. Duplicates show an average difference of 0.54% over all elements, indicating minimal error in sample preparation and analysis.

2.5 Estimation of Distribution Coefficients

The solid-water bulk distribution coefficient $D^{s/w}_i$ is defined as the concentration of element i in the solid C^s_i divided by that in the water C^w_i , both in ppm. $D^{s/w}$ values were estimated by analyzing water and solids collected at the same time and location. Only samples from rice paddies were included, as tidal channel water was rapidly flowing over tidal channel sediment and therefore unlikely to reach exchange equilibrium. Solid/extract $D^{s/e}_i$ values were estimated two ways. In the first, the measured bulk concentration of element i in the solid C^s_i was used with the measured concentration in the extract solution C^e_i , such that $D^{s/e}_i = C^s_i/C^e_i$. This assumes that the solid concentration was unaffected by equilibration with the extract solution. In the second method, the same information was used with mass balance to estimate the concentration in the residual solid C^{res}_i , which accounts for the amount of i that dissolved in the extract solution, as follows: $D^{s/e}_i = C^{res}_i/C^e_i$. Because measured $D^{s/e} \gg 10$ for all elements, the concentration in the solid did not change significantly even for soluble elements, so calculating $D^{s/e}$ using the two methods yielded nearly identical results, but the more accurate values estimated using mass balance were used. $D^{s/e}$ values were estimated for all solid types: tidal channel sediment, rice paddy soil, and Sundarbans soil.

3 Data

Sample site locations are shown in Fig. 1 and listed in Table 1. Element concentrations grouped by sample type are tabulated for water samples (Table 2), extracts (Table 3), and solids (Table 4). Concentrations of the elements Be, Cd, Pb, and Tl were frequently below our method detection limits, and so are not reported. Furthermore, our procedure for analyzing solids prevented us from measuring sample concentrations of elements that mainly form anions (since the 1% HNO_3 solution could not be introduced into the ion chromatograph) or were present in the flux (Li and B). Concentrations reported as negative were deleted. Although some positive concentrations for the remaining elements were below the method detection limit, we

manuscript submitted to *Geochemistry, Geophysics, Geosystems (G3)*
chose to use the data uncensored with no substitution, as removing concentrations below the detection limit would bias the results to higher concentrations. Sample types included tidal channel (TC), rice paddy (RP), and Sundarbans (SB). Some samples classified as “tidal channel” were from irrigation canals connected to tidal channels.

For water samples collected in the same season (dry season in May and wet season in November), and extracts prepared from solid samples collected in the same season, element concentrations were most often lognormally distributed, as was reported for water samples from the same region by Ayers et al. (2017). All statistical tests and plots therefore use \log_{10} values of concentrations. Although for solids many elements were not fit well by a lognormal distribution, we used a log transform on solid concentrations for consistency, and nonparametric statistical tests were used. Uncertainties are reported as one standard deviation (1σ).

Across sample sites, in-situ soil salinity slightly increased to the SE and with increasing proximity to the Bay of Bengal. In November, rice paddy water salinity slightly increased to the SSW. In general, soil and water salinity decrease to the North and with increasing distance from the coastline. Although the sampling area was $\sim 1300 \text{ km}^2$ (Fig. 1) and covered at least five different soil regions (Table 1), the variation in compositions of water and solid samples between sites was small within each season (e.g., Fig. S5), indicating similar processes are acting to transport elements across this region. We therefore lump data for all sites together in the following plots and discussion.

Values of specific conductivity (SpC), a proxy for salinity, of extracts were similar to in-situ solid conductivity measurements because the extract measurement was made on the solid slurry, not the filtered extract solution (Fig. 2). Salinity was much higher in solids and extracts than water samples (Fig. 2). Solids and extracts also show much less seasonality than water samples, which have higher salinity in the dry season.

To compare the wide range of element concentrations in solid, extract, and water, average concentrations were normalized to average upper continental crust (UCC) in spiderplots (Fig. 3) with elements arranged on the x-axis from lowest mobility during weathering and transport on the left to highest mobility on the right (Gaillardet et al., 2014). Tidal channel sediment (Fig. 3a) and rice paddy soil (Fig. 3b) are similar in

composition to average UCC but depleted in Ca, Sr, Na, As, and S. Extract and water samples show strong depletions in immobile elements and weak depletions in the mobile elements relative to solids. Extracts have higher concentrations than tidal channel and rice paddy water for most elements.

3.1 Water

In tidal channel water samples, variations in total dissolved solids (TDS) and SpC reflect variable contributions of seawater from the Bay of Bengal (Ayers et al., 2017). Calculated TDS in water samples ranged from 20 ppm in rainwater to as high as 20,276 ppm in May tidal channel samples. Tidal channel water has much higher salinity in the dry season than the wet season (Fig. 2). Previous studies have shown only small variations in water chemistry between tides, with salinity varying a maximum of 4 ppt depending on the location and time of year (Rahaman et al., 2014), much less than seasonal variations of ~20 ppt in our field area (Ayers et al., 2017). Wet season tidal channel and rice paddy water have similar salinity and element concentrations, consistent with observed irrigation of rice paddies with tidal channel water in the wet season (Ayers et al., 2017). In the dry season, most rice paddies have lower salinity than tidal channel water because they are irrigated with groundwater. Concentrations of conservative elements, which show a constant ratio with Cl concentrations, are consistent with these relationships inferred from salinity. Immobile elements such as Al, Fe, Zn, and Cr show little variation in concentration by season or location (as measured by the size of the error bars in Fig. 3), while redox sensitive elements such as Mn and S show larger variations (Table 2).

Saturation index calculations on seasonal average water compositions show that rice paddy and tidal channel waters are always saturated in hydroxyapatite, dolomite, muscovite, and the smectite mineral saponite, and usually saturated in quartz, illite, kaolinite, calcite, and K-feldspar. Dry season waters are also saturated in the smectite mineral beidellite.

3.2 Extracts

Like water, extracts show little variation in concentrations of immobile elements such as Al, Fe, Zn, Cr, and Ni by season or location (Table 3, Fig. 3). Soluble elements such as Na and redox sensitive elements such

as Mn and S show relatively large seasonal variations. Extracts from tidal channel sediments collected in the dry season generally have higher concentrations and SpC values than wet season extracts, though the same is not true for rice paddy samples. Extract pH was nearly always > 7.5 with little seasonal variation, consistent with the presence of carbonate minerals. Sundarbans and tidal channel sediment samples have higher extract TDS and SpC than rice paddies, suggesting that agricultural activity may flush out soluble salts (Fig. 2).

Comparison of sulfur in extracts measured as elemental S by ICP-OES and sulphate SO_4^{2-} measured by IC shows the two are highly correlated ($r = 0.997$). The median molar concentration was higher for S measured by ICP-OES at 6.4×10^{-4} than SO_4^{2-} measured by IC at 6.1×10^{-4} , suggesting a small portion was present as sulfide, and that most S is present as sulphate.

Saturation index calculations show that rice paddy soil and tidal channel sediment extracts are always saturated in hydroxyapatite and kaolinite, and usually saturated in illite, gibbsite, smectite minerals beidellite and saponite, and dolomite \pm quartz and calcite. Extracts are undersaturated in hydrous ferric oxyhydroxides that often control the mobility of arsenic and other elements in this region (Hossain et al., 2012). This may be due to their absence in the solids, to disequilibrium, or to their abundance being less than required to saturate the volume of extract solution.

3.3 Solids

The composition of sediment is strongly influenced by grain size (Garzanti et al., 2011). The laser granulometry-measured mode, median, and volume-weighted mean grain sizes for select solid samples from this study are given in Table 5. The average volume-weighted mean of rice paddy soils was 50 μm , tidal channel sediments 23 μm , and the single Sundarbans sample 48 μm . The median for the Sundarbans sample was 36 μm , similar to the 31 μm previously reported (Hale et al., 2019). Laser granulometry has been shown to overestimate the abundance of fine silt and clay-sized particles (Borromeo et al., 2019), so our samples may be coarser than the numbers indicate. We did not measure grain size distributions in enough samples to characterize spatial or seasonal variability. However, our limited measurements demonstrate that the sampled

solids are dominantly silt-sized and roughly comparable in size, although the rice paddy soil samples are slightly coarser than the tidal channel sediment samples. Our tidal channel sediment samples are likely finer because they were collected from the beds of irrigation canals connected to the surface of tidal channels. The lower flow velocity in the canals likely caused their bedload sediments to be finer than tidal channel bedload sediments and more similar to shallow tidal channel suspended sediments.

Powder x-ray diffraction was used to identify minerals in a tidal channel sediment sample and a rice paddy soil sample (Fig. 4). Quartz, illite, chlorite, biotite, and dolomite have multiple peaks in the 2θ range of $10-45^\circ$. Inspection of grain mounts with a polarizing microscope confirmed the presence of quartz, chlorite, and biotite. The minerals and their relative proportions assessed qualitatively by peak heights are very similar in tidal channel sediment and rice paddy soil. XRD analysis of clay minerals in four tidal channel sediment samples from Polder 32 (locations in Fig. S6) showed that illite and kaolinite were present in all samples, chlorite was present in two samples, and smectite was not present (Table S1). Other studies have shown that in Ganges River sediments illite is the most abundant clay, followed by smectite, kaolinite, and chlorite (MA Allison et al., 2003; Khan et al., 2019).

Compared to water and extracts, solid samples show less variation in element concentrations across seasons and sampling sites as measured by relative error bar size in Figs. 2 and 3 and comparison of mean concentrations in samples collected in May and November (Table 4). Our samples are from the distal portion of the Ganges basin, are fine-grained and therefore likely well-mixed, which would explain the small variance in element concentrations.

Average tidal channel sediment and rice paddy soil concentrations of immobile elements are similar to those of UCC (Fig. 5). Converting to oxide concentrations and normalizing to an anhydrous basis again shows the similarities to UCC, although FeO is lower and CaO and MgO higher than UCC, most likely due to sediment sorting (Table 6). However, major elements with intermediate mobilities including Ca, Sr, and Na are depleted, likely due to depletion of plagioclase feldspar through sedimentary sorting and/or chemical weathering (Garzanti et al., 2011; Lupker et al., 2012). This was also observed in Ganges bedload sand, which

manuscript submitted to *Geochemistry, Geophysics, Geosystems (G3)*
was found to be well-mixed (Garzanti et al., 2010). Mobile elements show variable behavior, with As and S being low relative to UCC.

Normalizing concentrations in rice paddy soil to tidal channel sediment highlights post-depositional changes in solid composition (Fig. 6). The only elements that show a substantial difference in concentration between rice paddy soil (C^{rp}) and tidal channel sediment (C^{tc}) were Na, with higher concentrations in May tidal channel sediment, and Si, which is higher in November rice paddy soil (Mann-Whitney test p values < 0.05). In both cases the 1σ error bars overlap with $\log_{10}C^{\text{rp}}/C^{\text{tc}} = 0$, indicating the differences in concentration are very small (Fig. 6).

4 Results

4.1 Element Correlations

Examination of element correlations can shed light on chemical processes. We found statistically significant correlations (p value for Pearson correlation coefficient < 0.05) for 166/276 element pairs in solids (e.g., Fig. S7), 160 of 406 element pairs in soil extracts (Figs. S8 and S9), and 285/378 pairs in water. Log concentrations of conservative elements such as Na, Cl, K, Mg, and Sr in extract solutions are normally distributed and are all positively correlated, consistent with simple dissolution of soluble salts (Fig. S8). The same is true for water samples collected in this region in this study and previous studies (Ayers et al., 2017). In contrast, conservative elements do not always show good correlations in bulk solids (Fig. S7), which have much higher concentrations of all elements (except S) than water or extracts (Fig. 3). This indicates that only a small portion of most cations are present in solids as soluble salts, and generally cations remain bound to solid minerals such as clays and Fe-Mn oxyhydroxides during extract preparation or exchange with standing water.

In contrast to conservative elements, log concentrations of nonconservative elements in water and extracts are not always normally distributed and can show positive, negative, or no correlation with other elements (Fig. S9). Arsenic shows a weak positive correlation with S in extracts, suggesting it may have been

present in sulfides. However, if sulfide oxidation occurred during extract preparation, it was insufficient to reduce pH to < 7 .

In bulk solids the metals Ba, Co, Cr, Cu, Fe, K, Mg, Mn, Na, Ni, Si, and Zn show strong ($r > 0.8$, $p < 0.05$) correlations with Al, indicating they may be stored in clay minerals or have similar sources. Arsenic has a strong positive correlation with Fe ($r = 0.78$, $p = 2.6\text{E-}6$), suggesting it may be sorbed onto hydrous ferric oxyhydroxides (HFOs) (Fendorf et al., 2010). In tidal channel and rice paddy water samples, most elements show positive correlations with TDS, reflecting variable amounts of seawater mixing, dilution, and evaporative concentration.

4.2 Element Partitioning

In soils and sediments, weathering reactions between porewaters and minerals will cause dissolution of primary minerals, precipitation of secondary minerals, and adsorption onto mineral surfaces. Trace elements can be incorporated into solids through adsorption, precipitation, or coprecipitation/substitution. The partitioning of trace element i incorporated into multi-phase solids by substitution can be described using the solid-water bulk distribution coefficient, which has the same form as the linear adsorption isotherm: $D^{s/w}_i = C^s_i / C^w_i$. For trace elements, a plot of concentrations in water versus solid should yield a linear array with a positive slope and a zero intercept if Henry's Law is obeyed and solid mineralogy does not change, and the slope should equal the value of the trace element distribution coefficient $D^{s/w}$. This should be true regardless of whether the element is incorporated in solids by coprecipitation (substitution) or adsorption. While D values should be constant only for trace elements, they are still useful for evaluating whether major elements partition more strongly into solid or solution. $D^{s/w}$ values were calculated only for samples of water and rice paddy soil collected at the same time and location (Table S2). $D^{s/e}$ values were calculated for extracts prepared from the same rice paddy soil or tidal channel sediment sample (Table S3). D values are roughly lognormally distributed for each element. For most elements, $D^{s/w}$ values are similar to $D^{s/e}$ values (Fig. 7). D values calculated from average concentrations in Tables 2-4 are similar to averages from paired samples, suggesting our results are robust and not site-specific.

Inter-element variances are larger than intra-element variances, suggesting that D values represent relative element mobilities (Fig. 7). Also, intra-element variances are relatively small, considering that samples were collected at different locations, time of year, and time of day.

We observed poor and often negative correlations between concentrations of an element in solid and water or extract. The poor correlations may result from variable water compositions (especially pH) and solid mineralogies, although these would not likely cause negative correlations between concentrations in solids and aqueous solutions. Another potential explanation is disequilibrium partitioning. This is supported by seasonal changes in composition that are large for water and small for soil. From the dry season in May to the wet season in November, metal concentrations in soil and sediment change little (Fig. 5, larger error bars in Fig. 3 for water than for solids), despite surface water compositions changing dramatically from saline to fresh (Fig. 2). The average percentage seasonal difference in element concentrations were 147% and 13% for water and soil, respectively. Disequilibrium exchange is also supported by a lack of systematic dependence on pH, which should strongly affect mineral solubilities and adsorption of dissolved ions, and by the oversaturation of many minerals in extract solutions, including quartz. Also, the 15 minutes that the solid and extract solution remained in contact (the recommended duration for soil extracts cf. Tan (2005)) was likely insufficient to reach exchange equilibrium. Previous studies have shown that while > 75% of metal adsorption in batch experiments occurred within the first 30 minutes, some metals could take up to 300 minutes to reach a steady state solution concentration (Zhang et al., 2019).

While our measured distribution coefficients cannot be considered equilibrium D values, they are still useful as measures of element mobility, with low D values indicating high element mobility (Gaillardet et al., 2014). For sediments and soils in this region that have similar mineralogy, our D values can be used to estimate concentrations in solids from concentrations in standing water or extracts, which are easier to measure. This would be particularly useful for estimating concentrations of toxic elements such as As in agricultural soils.

As expected, D values are highest for the least mobile elements Al and Fe, and lowest for the most mobile element S (Fig. 7). Based on the mobility ranking (the order of elements on the x-axis), D is higher for

Si and lower for Ca, Sr, and Na than expected. The higher D for Si is probably due to the relatively high proportion of quartz in the silt-sized sediments and soil (Fig. 4), while low D values for Ca, Sr, and Na likely result from removal of plagioclase feldspar by sedimentary sorting and/or weathering.

4.3 Sediment and Soil Compositions

Chemical weathering during transport and following sediment deposition converts primary minerals into dissolved solutes and secondary minerals, which changes the chemical compositions of solids and fluids. Weathering of sediments causes the following changes in mineralogy of sediments/soils and major element compositions of fluids: conversion of albite and K-feldspar to kaolinite or smectite releases Na and K respectively; conversion of biotite to vermiculite releases K; and calcite and dolomite dissolution release Ca and Mg (Lupker et al., 2012). Previous work has shown that progressive weathering of sediments near the Himalayan Front and the Ganges floodplain depletes sediments in the mobile elements that are released by weathering reactions (Lupker et al., 2012), particularly elements released by soluble minerals such as carbonates that dissolve rapidly. As a result, alkalis and alkaline earths in the suspended load of the Ganges River are depleted relative to UCC, even in the upper reaches of the Ganges Basin (Garzanti et al., 2011). We also observe depletion in alkaline earths like Ca and Sr and alkalis like Na, which could be caused by the removal of low-density plagioclase feldspar and its Na and Ca components by chemical weathering (Fig. 5, Table 5, lack of plagioclase feldspar in x-ray diffraction patterns in Fig. 4). In contrast, tidal channel sediments and rice paddy soils both show enrichment in K relative to UCC (Table 5), probably due to illite being the most abundant clay mineral (Fig. 4).

Suspended sediments in unpolluted large river systems such as the Ganges have compositions very similar to average UCC (Gaillardet et al., 2014). This explains why our sediment and soil samples from the Ganges tidal plain, which were derived from suspended sediments, have trace element compositions very similar to average UCC (Fig. 3). Only a few elements are depleted relative to UCC, those in the dissolved load and those concentrated in heavy minerals in the bedload. No elements are enriched relative to UCC, indicating

no significant anthropogenic inputs. Plotting only solids highlights small differences between trace element concentrations in solids and UCC (Fig. 5). Compared to rice paddy soils and tidal channel sediments, normalized concentrations of many trace elements in Sundarbans soils are higher in the wet season and lower in the dry season (Fig. 5), although we have only one sample each of wet and dry season Sundarbans soils (cf. Table 4).

Poldering in coastal Bangladesh has greatly reduced the frequency of tidal flooding and sediment deposition. On Polder 32, the last significant sediment deposition event started with Cyclone Aila in 2009 and ended after embankment repairs were completed in 2010 (Auerbach et al., 2015). After roughly seven years, element concentrations in Polder 32 rice paddy soil are only slightly different from tidal channel sediment (Fig. 8), indicating little effect of in-situ chemical weathering.

Rice paddy soil and tidal channel sediment have similar mineralogy (Fig. 4), major element compositions (Table 6), and trace element compositions (Figs. 6 and 8). These similarities can only occur if two conditions are met: sediments deposited inside the polder are similar in composition to sediments deposited in the tidal channels/irrigation canals; and the influence of post-depositional weathering on mineralogy and composition is insignificant. Sediment deposition within polders occurred either before embankments were constructed in the 1960s or during tidal inundation following embankment breaches (Auerbach et al., 2015). None of the sampled areas have been affected by tidal river management, which involves deliberate flooding to induce sedimentation and an increase in land elevation to reduce waterlogging (Gain, 2017). Tidal inundation would cause deposition of silt-sized suspended sediments and not sand-sized bedload sediments within a polder, since silt is the dominant grain size in suspended sediments of most rivers (Garzanti et al., 2011), and is the dominant grain size in tidal channel sediments and polder soils within the study area (Table 5). Since polder soils have grain size distributions, mineralogies, and compositions similar to sediments deposited in tidal channels (although the measured polder soils were slightly coarser cf. Table 5), the effects of post-depositional chemical weathering within the polders have been insignificant.

An alternative explanation is that since our tidal channel sediment samples were actually collected mostly from irrigation canals, the rice paddy soils are actually sediments deposited from irrigation water, and that this process is continuous. This could explain why our rice paddy soil and tidal channel sediment samples have similar mineralogies and compositions. However, our RP soil is coarser than the TC sediment, and if it was deposited by irrigation water, it would be finer. Furthermore, water in the irrigation canals moves very slowly due to miniscule changes in elevation, so that water entering rice paddies has near zero suspended sediment. If sediment deposition from irrigation water was significant, then irrigation canals would quickly clog with sediment, and rice paddies would be at higher elevation than adjacent land, neither of which was observed. Finally, a trench dug into surficial sediments inside Polder 32 showed that all near-surface sediment showed tidal laminations, indicating sediment was deposited during tidal inundation following Hurricane Aila and not from irrigation water.

A larger Bangladesh dataset of soil samples collected throughout Bangladesh showed that element concentrations in paddy and non-paddy soils are positively correlated and similar (M. T. A. Chowdhury et al., 2017). Linear regression of element concentrations in non-paddy versus paddy soils yielded a slope of less than one for all elements but arsenic, indicating that only arsenic was added to paddy soils by irrigation (M. T. A. Chowdhury et al., 2017). It is unclear whether the non-paddy soils in that study are comparable to tidal channel sediments in this study, but both studies demonstrate that the influence of rice paddy agriculture on soil composition in Bangladesh is small.

4.4 Chemical Weathering

Our results suggest that element concentrations change more slowly in solids than in surface water as seasons change. Water-solid exchange rates must be too slow for solids to equilibrate with surface waters, which have short residence times and experience seasonal changes in composition. Solid exchange was also too slow to significantly modify the composition of the top 15 cm of soil on Polder 32 during the seven years

between sediment deposition after Cyclone Aila in 2009 and our collection of rice paddy soils in 2016 (Fig. 8), although we see seasonal changes in concentrations of some elements, especially soluble salts (Table 4).

As discussed in Section 1.2, the average age of the top 15 cm at sites other than Polder 32 is estimated at ~7.5 years since deposition after Hurricane Aila in 2009 and sample collection in 2016. For polders other than Polder 32 that we collected samples from, it is possible that embankment breaches occurred during Hurricane Aila, but unlikely that they occurred after Aila and before sample collection. If Aila did not cause embankment breaches in these polders, then collected soil samples would be older than 7.5 years, since sedimentation rates in the region have decreased since poldering in the 1960s, but not by more than a few decades. During that time, chemical weathering had little effect on the composition of rice paddy soils at any of the investigated sites, indicating that the rate of chemical weathering is very low.

Garzanti et al. (2019) assert that $\alpha^{\text{AlNa}} = [\text{Al/Na}]_{\text{sample}}/[\text{Al/Na}]_{\text{UCC}}$ is the chemical index most sensitive to weathering because it is affected by the weathering of relatively unstable Na-rich plagioclase feldspar. They give values for Ganges River suspended sediments of 4.2 for shallow load and 2.4 for deep load, compared with Brahmaputra River suspended sediments of 2.4 shallow and 1.7 deep. These values are consistent with previous work that showed that sediments in the Ganges floodplain, which have longer storage times, are more intensely weathered than sediments in the Brahmaputra floodplain (Garzanti et al., 2019). Our samples give average $\alpha^{\text{AlNa}} \sim 2.2$ for rice paddy soil and 1.8 for tidal channel sediment, indicating that measurable weathering has occurred. Our values are closer to Brahmaputra than Ganges suspended load, which may indicate a tidal input of Brahmaputra sediments from the shelf. However, Sr concentrations of < 100 ppm in tidal channel sediments and rice paddy soils are consistent with a solely Ganges provenance (Table 4, Goodbred et al., 2014).

The small changes in solid compositions across our field sites is mirrored by small changes in November tidal channel water compositions between upstream (4 samples from sites B3, B8, and B9) and downstream locations (4 samples from sites P32, B2, and SB), which are separated by ~ 50 km (Fig. 9). While changes in element discharge (solute fluxes) are needed to estimate the contribution from chemical weathering, the water discharge likely changes little over this 50 km stretch, so a small change in element concentrations is equivalent

to low solute fluxes, which is consistent with low chemical weathering inputs. This is also supported by previous work in this region that found concentrations of conservative elements such as Na, Mg, Sr, and Cl in surface waters are explained by simple mixing of rainwater and seawater, with no contributions from chemical weathering (Ayers et al., 2017). The evidence suggests that most or all dissolved solutes in tidal channel water in the study area are derived from other areas, including the fluvial-dominated delta upstream and the Bay of Bengal downstream, and that chemical weathering inputs to tidal channels in the study area are low.

Far upstream in the Ganges River Basin, in the Himalaya and the alluvial fan, weathering is rapid because exhumation and erosion provide a continuous supply of fresh sediments. In this weathering-limited regime in the headwaters of the Ganges, dissolved and suspended sediment fluxes increase downstream, and river sediments show continuous downstream increases in the Chemical Index of Alteration and decreases in Th activity ratios and U/Th caused by chemical weathering (Granet et al., 2007). River waters in the upper reaches are less likely to be calcite-saturated than in the lower reaches (Sarin et al., 1989), while solute concentrations increase downstream from the alluvial fan before leveling off (Bickle et al., 2018). Sediment may be weathered during transport as it works its way through the alluvial fan (Stallard & Edmond, 1983), although evidence from the east African rift shows that the amount of weathering in the alluvial fan may be small even in hot, humid climates due to rapid transport (Garzanti et al., 2013). Far upstream of our study area at Farraka, India, just upstream of Harding Bridge (Fig. 1), changes in Ganges River dissolved solute fluxes indicate that floodplain weathering contributes roughly half of major dissolved cation fluxes (Bickle et al., 2018), consistent with estimates based on sediment composition (Lupker et al., 2012).

In contrast, in transport-limited areas the rate of chemical weathering is limited by the rate of supply of fresh material, and is lower than in the weathering-limited regime (Bickle et al., 2018; West et al., 2005). Our data suggest that a transport-limited regime prevails in the lower reaches of the Ganges Basin, consistent with predictions of a transition from weathering-limited regimes in highlands to transport-limited regimes in lowlands (Bickle et al., 2018; Gaillardet et al., 1999). In the lower river reaches, such as the tidal delta plain where our sampling sites are located, the solid material is more weathered than the fresh material in the alluvial

fan. Unstable primary minerals have mostly been replaced by stable, cation-depleted secondary minerals such as clays, consistent with our observed sample mineralogies being dominated by clay minerals and relatively stable minerals such as quartz (Fig. 4).

In the Ganges lowlands, water residence times are longer than in the highlands, especially in the floodplain. Chemical weathering is typically transport-limited in soils, which have moderate fluid residence times of 5 days to 10 years (Maher, 2010). Tidal channel water that is used for irrigating rice paddy soils has high dissolved solids (Table 2, Ayers et al., 2017), which lowers the chemical weathering rates of minerals. Water samples from rice paddies and tidal channels are saturated in the dominant minerals observed in our solid samples (illite, dolomite, kaolinite) and minerals that commonly occur in sediments in the lower reaches of the Ganges River basin such as smectites, indicating that these minerals will not dissolve in the waters their host solids come in contact with. These waters are even saturated in primary minerals such as K-feldspar, muscovite, and hydroxyapatite. The only unstable mineral we identified that is undersaturated in surface waters is biotite. Extract solutions, which are likely more similar to soil porewater compositions than standing water in rice paddies, are even more concentrated in dissolved solutes, and saturated in the same minerals. That water samples are already saturated in most of the minerals they would come in contact with (the stable minerals quartz, kaolinite, illite) is strong evidence that the driving force for chemical weathering is low.

Solids will not change in composition or mineralogy if the weathering agent water is already in equilibrium with the minerals. This is consistent with the small changes in the compositions of soil over time (as compared with fresh tidal channel sediment) and of tidal river water across our study area. Somewhere between our downstream study area and Harding Bridge upstream must be the transition from weathering-dominated to transport-dominated regimes. For the main stem Ganges, the transition may be located near the break in river slope that separates the alluvial fan from the fluvial-tidal delta plain and causes a decrease in water velocity and average grain size downstream (Wilson & Goodbred, 2015).

While measurable chemical weathering occurred upstream of our sample sites (Bickle et al., 2018; Lupker et al., 2012), no evidence of chemical weathering was detected within our study area. Our data show

that the chemical weathering rate in the tidal delta plain is low, which is more consistent with a transport-limited regime than a weathering-limited regime. The area of the delta in the transport-limited regime should increase with factors that increase the rate of chemical weathering such as temperature and runoff (West et al., 2005). Since both of these factors are high in the GBM delta, it seems likely that the entire tidal delta plain is in the transport-limited regime.

While the dearth of unstable minerals and higher solute loads in the tidal delta plain decrease the Gibbs Free Energy change and rates of chemical weathering reactions, the lack of systematic partitioning (and the oversaturation in many minerals) shows that solids and surface waters are not in chemical equilibrium. Solids show little seasonal variation in composition, while surface waters show large variations. Disequilibrium between standing water and the top 15 cm of sediment and soil may result from the solids being dominated by swelling clays such as smectites that are abundant in the Ganges clay-sized fraction (Borromeo et al., 2019) and that make surface deposits impermeable (Benson et al., 1994). Swelling will occur in the wet season due to abundant water for interlayer sites in smectites such as beidellite, while in the dry season abundant Na^+ may displace Ca^{2+} and Mg^{2+} and cause swelling (Langmuir, 1997). Swelling clays may therefore inhibit chemical weathering reactions in the soil.

5 Conclusions

Rice paddy soil and tidal channel sediment in the Ganges tidal plain in SW Bangladesh have similar mineralogies and compositions. Since soils formed from tidal channel sediments deposited at least 7.5 years ago, the lack of change in composition during that time indicates low rates of chemical weathering, which would be consistent with a transport-limited regime. Longer periods of near-surface exposure would be needed to quantify the low chemical weathering fluxes in this region. Rice paddy and tidal channel waters are saturated in the dominant minerals present in soils and sediments, indicating low Gibbs Free Energy changes and rates of weathering reactions.

Tidal channel sediment and rice paddy soil show little or no seasonal variation in composition. In contrast, the composition of water in rice paddies and tidal channels does vary seasonally, with wet season samples being more dilute. This suggests that compositions of solids change more slowly than solutions, which explains much of the intra-element variation in our measured apparent solid/water distribution coefficients. While measured distribution coefficients are not equilibrium values, the relative values for the elements studied are mostly consistent with previously published trends of element mobility during weathering and transport (Gaillardet et al., 2014). Disequilibrium partitioning between fine-grained sediments and surface waters may be a common feature in river deltas due to the presence of swelling clays, the low supply of unweathered material, and saturation of most available minerals in water, which together keep chemical weathering rates low.

Acknowledgments, Samples, and Data

The authors have no financial conflicts of interest related to this paper. Thanks to Steve Goodbred for advice, Rossane DeLapp for quickly analyzing our samples, Carol Wilson for collecting the samples analyzed for clay mineralogy, Md Nazrul Islam (Bachchu) from Pugmark Tours, Saddam Hossain from Dhaka University, and Chelsea Peters from Vanderbilt University for help in the field. We appreciate the thorough reviews by Eduardo Garzanti and an anonymous reviewer. Any opinions, findings, conclusions, or recommendations expressed in this material are those of the authors and do not necessarily reflect the views of the National Science Foundation.

Research Data associated with this article can be accessed at <http://dx.doi.org/10.17632/6z6bdxrkbb.2>

References

- Allison, M., & Kepple, E. (2001). Modern sediment supply to the lower delta plain of the Ganges-Brahmaputra River in Bangladesh. *Geo-Marine Letters*, 21(2), 66–74. <https://doi.org/10.1007/s003670100069>
- Allison, MA, Khan, S., Goodbred, S., & Kuehl, S. (2003). Stratigraphic evolution of the late Holocene Ganges–Brahmaputra lower delta plain. *Sedimentary Geology*, 155, 317–342. [https://doi.org/10.1016/S0037-0738\(02\)00185-9](https://doi.org/10.1016/S0037-0738(02)00185-9)
- Auerbach, L. W., Goodbred Jr, S. L., Mondal, D. R., Wilson, C. A., Ahmed, K. R., Roy, K., et al. (2015). Flood risk of natural and embanked landscapes on the Ganges–Brahmaputra tidal delta plain. *Nature Climate Change*, 5(2), 153–157. <https://doi.org/10.1038/nclimate2472>
- Ayers, J. C., Goodbred, S., George, G., Fry, D., Hornberger, G., Benneyworth, L., et al. (2016). Sources of salinity and arsenic in groundwater in southwest Bangladesh. *Geochemical Transactions*, 17(4), 1–22. <https://doi.org/10.1186/s12932-016-0036-6>
- Ayers, J. C., George, G., Fry, D., Benneyworth, L., Wilson, C., Auerbach, L., et al. (2017). Salinization and arsenic contamination of surface water in southwest Bangladesh. *Geochemical Transactions*, 18(1), 4. <https://doi.org/10.1186/s12932-017-0042-3>
- Barmon, B. K., Kondo, T., & Osanami, F. (2010). Rice-prawn Farming System: Impacts on Soil Quality and Land Productivity of Modern Variety Paddy Production in Bangladesh. *Asian Journal of Agriculture and Development*, 7(2), 49–66. Retrieved from [http://beta.searca.org/searca/ajad/files/101111132631_Barmon, Kondo, Yamaguchi, and Osanami.pdf](http://beta.searca.org/searca/ajad/files/101111132631_Barmon,Kondo,Yamaguchi,andOsanami.pdf)
- Benneyworth, L., Gilligan, J., Ayers, J., Goodbred, S., George, G., Carrico, A., et al. (2016). Drinking water insecurity: water quality and access in coastal south-western Bangladesh. *International Journal of Environmental Health Research*, 26. <https://doi.org/10.1080/09603123.2016.1194383>

Benson, C. H., Huaming, Z., & Xiaodong, W. (1994). Estimating Hydraulic Conductivity of Compacted Clay Liners. *Journal of Geotechnical Engineering*, 120(2), 366–387. [https://doi.org/10.1061/\(ASCE\)0733-9410\(1994\)120:2\(366\)](https://doi.org/10.1061/(ASCE)0733-9410(1994)120:2(366))

Bethke, C. M. (2007). *Geochemical and biogeochemical reaction modeling*. Cambridge University Press.

Bickle, M. J., Chapman, H. J., Tipper, E., Galy, A., De La Rocha, C. L., & Ahmad, T. (2018). Chemical weathering outputs from the flood plain of the Ganga. *Geochimica et Cosmochimica Acta*, 225, 146–175. <https://doi.org/https://doi.org/10.1016/j.gca.2018.01.003>

Biscaye, P. E. (1965). Mineralogy and Sedimentation of Recent Deep-Sea Clay in the Atlantic Ocean and Adjacent Seas and Oceans. *Geological Society of America Bulletin*, 76, 803. [https://doi.org/10.1130/0016-7606\(1965\)76\[803:MASORD\]2.0.CO;2](https://doi.org/10.1130/0016-7606(1965)76[803:MASORD]2.0.CO;2)

Bomer, E. J., Wilson, C. A., Hale, R. P., Hossain, A. N. M., & Rahman, F. M. A. (2020). Surface elevation and sedimentation dynamics in the Ganges-Brahmaputra tidal delta plain, Bangladesh: Evidence for mangrove adaptation to human-induced tidal amplification. *CATENA*, 187, 104312. <https://doi.org/https://doi.org/10.1016/j.catena.2019.104312>

Borromeo, L., Andò, S., France-lanord, C., Coletti, G., Hahn, A., & Garzanti, E. (2019). Provenance of Bengal Shelf Sediments: 1. Mineralogy and Geochemistry of Silt. *Minerals*, 9(10), 640. <https://doi.org/10.3390/min9100640>

Brammer, H. (2012). *The Physical Geography of Bangladesh*. The University Press Ltd.

Brammer, Hugh. (2016). *Bangladesh: Landscapes, soil fertility and climate change*. Dhaka, Bangladesh: The University Press Limited.

Chen, L.-M., Zhang, G.-L., & Effland, W. R. (2011). Soil characteristic response times and pedogenic thresholds during the 1000-year evolution of a paddy soil chronosequence. *Soil Science Society of America*

- Chowdhury, M. T. A., Deacon, C. M., Jones, G. D., Imamul Huq, S. M., Williams, P. N., Manzurul Hoque, A. F. M., et al. (2017). Arsenic in Bangladeshi soils related to physiographic region, paddy management, and micro- and macro-elemental status. *Science of the Total Environment*.
<https://doi.org/10.1016/j.scitotenv.2016.11.191>
- Chowdhury, N. T. (2010). Water management in Bangladesh: an analytical review. *Water Policy*, 12(1), 32.
<https://doi.org/10.2166/wp.2009.112>
- Edmond, J. M. (1992). Himalayan Tectonics, Weathering Processes, and the Strontium Isotope Record in Marine Limestones. *Science*, 258(5088), 1594 LP – 1597. <https://doi.org/10.1126/science.258.5088.1594>
- Fendorf, S., Michael, H. A., & van Geen, A. (2010). Spatial and temporal variations of groundwater arsenic in South and Southeast Asia. *Science*, 328(5982), 1123–7. <https://doi.org/10.1126/science.1172974>
- Fry, D. C. (2015). *Characterizing temporal and spatial trends in soil geochemistry on Polder 32, Southwest Bangladesh*. Vanderbilt University. Retrieved from <http://etd.library.vanderbilt.edu/available/etd-07162015-214524/>
- Gaillardet, J., Dupré, B., Louvat, P., & Allègre, C. J. (1999). Global silicate weathering and CO₂ consumption rates deduced from the chemistry of large rivers. *Chemical Geology*, 159(1), 3–30.
[https://doi.org/https://doi.org/10.1016/S0009-2541\(99\)00031-5](https://doi.org/https://doi.org/10.1016/S0009-2541(99)00031-5)
- Gaillardet, J., Viers, J., & Dupré, B. (2014). Trace Elements in River Waters. In H. D. Holland & K. K. B. T. Turekian (Eds.), *Treatise on Geochemistry* (2nd ed., pp. 195–235). Oxford: Elsevier. <https://doi.org/https://doi.org/10.1016/B978-0-08-095975-7.00507-6>
- Gain, A. K., Benson, D., Rahman, R., Datta, D. K., & Rouillard, J. J. (2017). Tidal river management in the south west Ganges-Brahmaputra delta in Bangladesh: Moving towards a transdisciplinary approach?

<https://doi.org/10.1016/j.envsci.2017.05.020>

- Gandois, L., Perrin, A.-S., & Probst, A. (2011). Impact of nitrogenous fertiliser-induced proton release on cultivated soils with contrasting carbonate contents: A column experiment. *Geochimica et Cosmochimica Acta*, 75(5), 1185–1198. <https://doi.org/10.1016/j.gca.2010.11.025>
- Garzanti, E., Andò, S., France-Lanord, C., Vezzoli, G., Censi, P., Galy, V., & Najman, Y. (2010). Mineralogical and chemical variability of fluvial sediments 1. Bedload sand (Ganga-Brahmaputra, Bangladesh). *Earth and Planetary Science Letters*, 299(3–4), 368–381. <https://doi.org/10.1016/j.epsl.2010.09.017>
- Garzanti, E., Andó, S., France-lanord, C., Censi, P., Vignola, P., Galy, V., & Lupker, M. (2011). Mineralogical and chemical variability of fluvial sediments 2. Suspended-load silt (Ganga–Brahmaputra, Bangladesh). *Earth and Planetary Science Letters*, 302(1–2), 107–120. <https://doi.org/10.1016/j.epsl.2010.11.043>
- Garzanti, E., Padoan, M., Andò, S., Resentini, A., Vezzoli, G., & Lustrino, M. (2013). Weathering and Relative Durability of Detrital Minerals in Equatorial Climate: Sand Petrology and Geochemistry in the East African Rift. *The Journal of Geology*, 121(6), 547–580. <https://doi.org/10.1086/673259>
- Garzanti, E., Vezzoli, G., Andò, S., Limonta, M., Borromeo, L., & France-Lanord, C. (2019). Provenance of Bengal Shelf Sediments: 2. Petrology and Geochemistry of Sand. *Minerals*, 9(10), 642. <https://doi.org/10.3390/min9100642>
- Goodbred, S. L., Paolo, P. M., Ullah, M. S., Pate, R. D., Khan, S. R., Kuehl, S. a., et al. (2014). Piecing together the Ganges-Brahmaputra-Meghna River delta: Use of sediment provenance to reconstruct the history and interaction of multiple fluvial systems during Holocene delta evolution. *Geological Society of America Bulletin*, 126(11), 1495–1510. <https://doi.org/10.1130/B30965.1>
- Granet, M., Chabaux, F., Stille, P., France-Lanord, C., & Pelt, E. (2007). Time-scales of sedimentary transfer

manuscript submitted to *Geochemistry, Geophysics, Geosystems (G3)*
and weathering processes from U-series nuclides: Clues from the Himalayan rivers. *Earth and Planetary
Science Letters*, 261(3), 389–406. <https://doi.org/https://doi.org/10.1016/j.epsl.2007.07.012>

Hale, R. P., Wilson, C. A., & Bomer, E. J. (2019). Seasonal Variability of Forces Controlling Sedimentation in the Sundarbans National Forest, Bangladesh. *Frontiers in Earth Science*, 7, 1–13.
<https://doi.org/10.3389/feart.2019.00211>

Horneman, A., van Geen, A., Kent, D. V., Mathe, P. E., Zheng, Y., Dhar, R. K., et al. (2004). Decoupling of As and Fe release to Bangladesh groundwater under reducing conditions. Part I: Evidence from sediment profiles1 1Associate editor: G. Sposito. *Geochimica et Cosmochimica Acta*, 68(17), 3459–3473.
<https://doi.org/https://doi.org/10.1016/j.gca.2004.01.026>

Hossain, M., Williams, P. N., Mestrot, A., Norton, G. J., Deacon, C. M., & Meharg, A. A. (2012). Spatial heterogeneity and kinetic regulation of arsenic dynamics in mangrove sediments: The Sundarbans, Bangladesh. *Environmental Science and Technology*, 46(16), 8645–8652.
<https://doi.org/10.1021/es301328r>

Islam, M. A., Al-Mamun, A., Hossain, F., Quraishi, S. B., Naher, K., Khan, R., et al. (2017). Contamination and ecological risk assessment of trace elements in sediments of the rivers of Sundarban mangrove forest, Bangladesh. *Marine Pollution Bulletin*, 124(1), 356–366.

Khan, M. H. R., Liu, J., Liu, S., Seddique, A. A., Cao, L., & Rahman, A. (2019). Clay mineral compositions in surface sediments of the Ganges-Brahmaputra-Meghna river system of Bengal Basin, Bangladesh. *Marine Geology*, 412, 27–36. <https://doi.org/https://doi.org/10.1016/j.margeo.2019.03.007>

Langmuir, D. (1997). *Aqueous Environmental Geochemistry*. Upper Saddle River, NJ: Prentice Hall.

Lupker, M., France-Lanord, C., Galy, V., Lavé, J., Gaillardet, J., Gajurel, A. P., et al. (2012). Predominant floodplain over mountain weathering of Himalayan sediments (Ganga basin). *Geochimica et*

- Maher, K. (2010). The dependence of chemical weathering rates on fluid residence time. *Earth and Planetary Science Letters*, 294(1), 101–110. <https://doi.org/https://doi.org/10.1016/j.epsl.2010.03.010>
- Milliman, J. D., & Farnsworth, K. L. (2013). *River Discharge to the Coastal Ocean: A Global Synthesis*. Cambridge University Press (Vol. 24). <https://doi.org/10.5670/oceanog.2011.108>
- Naus, F. L., Schot, P., Ahmed, K. M., & Griffioen, J. (2019). Influence of landscape features on the large variation of shallow groundwater salinity in southwestern Bangladesh. *Journal of Hydrology X*, 5(October). <https://doi.org/10.1016/j.hydroa.2019.100043>
- Pansu, M., & Gautheyrou, J. (2007). *Handbook of soil analysis: mineralogical, organic and inorganic methods*. Springer Science & Business Media.
- Patton, B. (2018). *The Effect of Irrigation Source on Arsenic and Salt Concentrations in Soil in Southwest Bangladesh*. Vanderbilt University.
- Pickering, J. L., Goodbred, S. L., Beam, J. C., Covey, A. K., Ayers, J., Rajapara, H. M., & Singhvi, A. K. (2017). Terrace formation in the upper Bengal basin since the Middle Pleistocene: Brahmaputra fan delta construction during multiple highstands. *Basin Research*, 1–18. <https://doi.org/10.1111/bre.12236>
- R Core Team. (2019). *R: A Language and Environment for Statistical Computing*. Vienna, Austria: R Foundation for Statistical Computing.
- Rahaman, S. M. B., Biswas, S. K., Rahaman, M. S., Ghosh, A. K., Sarder, L., Siraj, S. M. S., & Islam, S. S. (2014). Seasonal nutrient distribution in the Rupsha-Passur tidal river system of the Sundarbans mangrove forest, Bangladesh. *Ecological Processes*, 3(1), 18. <https://doi.org/10.1186/s13717-014-0018-5>
- Raymo, M. E., & Ruddiman, W. F. (1992). Tectonic forcing of late Cenozoic climate. *Nature*, 359(6391), 117–

- Rogers, K. G., Goodbred, S. L., & Mondal, D. R. (2013). Monsoon sedimentation on the “abandoned” tide-influenced Ganges-Brahmaputra Delta plain. *Estuarine, Coastal and Shelf Science*, 131, 297–309.
- Sarin, M. M., Krishnaswami, S., Dilli, K., Somayajulu, B. L. K., & Moore, W. S. (1989). Major ion chemistry of the Ganga-Brahmaputra river system: Weathering processes and fluxes to the Bay of Bengal. *Geochimica et Cosmochimica Acta*, 53(5), 997–1009. [https://doi.org/https://doi.org/10.1016/0016-7037\(89\)90205-6](https://doi.org/10.1016/0016-7037(89)90205-6)
- Singh, M., Müller, G., & Singh, I. B. (2003). Geogenic distribution and baseline concentration of heavy metals in sediments of the Ganges River, India. *Journal of Geochemical Exploration*, 80(1), 1–17.
- Stallard, R. F., & Edmond, J. M. (1983). Geochemistry of the Amazon: 2. The influence of geology and weathering environment on the dissolved load. *Journal of Geophysical Research: Oceans*, 88(C14), 9671–9688. <https://doi.org/10.1029/JC088iC14p09671>
- Tan, K. H. (2005). *Soil sampling, preparation, and analysis*. CRC.
- West, A. J., Galy, A., & Bickle, M. (2005). Tectonic and climatic controls on silicate weathering. *Earth and Planetary Science Letters*, 235(1), 211–228. [https://doi.org/https://doi.org/10.1016/j.epsl.2005.03.020](https://doi.org/10.1016/j.epsl.2005.03.020)
- White, A. F., & Buss, H. L. (2014). Natural weathering rates of silicate minerals. In *Treatise on Geochemistry, Second Edition*. Elsevier, Oxford (pp. 115–155).
- Wilson, C. A., & Goodbred, S. L. (2015). Construction and maintenance of the Ganges-Brahmaputra-Meghna delta: Linking process, morphology, and stratigraphy. *Annual Review of Marine Science*, 7, 67–88. <https://doi.org/10.1146/annurev-marine-010213-135032>
- Zhang, J., Wang, X., Zhu, Y., Huang, Z., Yu, Z., Bai, Y., et al. (2019). The influence of heavy metals in road

manuscript submitted to *Geochemistry, Geophysics, Geosystems (G3)*
dust on the surface runoff quality: Kinetic, isotherm, and sequential extraction investigations.

Ecotoxicology and Environmental Safety, 176(March), 270–278.

<https://doi.org/10.1016/j.ecoenv.2019.03.106>

Figure Captions

Figure 1. Map of solid sample collection locations specified as Site_Sample #_Sample type. Water samples were collected from the same locations. The sample types are RP rice paddy, TC tidal channel, and SB Sundarbans. Detailed site maps are given in Figures S1-S4. The basemap is ESRI's world topographic map.

Figure 2. Boxplot comparing \log_{10} of specific conductivity SpC in mS/cm of samples classified by group (rice paddy soil RP, Sundarbans SB, and tidal channel sediment TC), month (dry season May = 5, wet season November = 11), and sample type. In-situ solid SpC measurements were not made in May.

Figure 3. Average compositions of all solid, extract, and water samples normalized to average upper continental crust (Rudnick & Gao, 2003). The one standard deviation error bars represent the variability across sites, sample types, and season. Elements are arranged on the x-axis from lowest mobility during weathering and transport on the left to highest mobility on the right (Gaillardet et al., 2014). a) Tidal channel samples, n = 12 extract, 13 solid, and 13 water samples. b) Rice paddy samples, n = 32 extract, 30 solid, and 48 water samples. The red horizontal line represents average upper continental crust.

Figure 4. Powder x-ray diffraction patterns for rice paddy soil sample BEMS_08_RPS_06M_May in red and tidal channel sediment sample BEMS_03_TC_01_May in blue. The y-axis is observed intensity and is truncated for visualization.

Figure 5. Average compositions of rice paddy soil, Sundarbans soil, and tidal channel sediment in May and November. The horizontal red line represents average upper continental crust (Rudnick and Gao, 2003).

Figure 6. Concentration in rice paddy soil Crp normalized to concentration in tidal channel sediment

Ctc by sample collection month, plotted as log values with one sigma error bars.

Figure 7. Log₁₀ D values for solid/extract $D^{s/e}$ and solid/water $D^{s/w}$ with one sigma error bars. $D^{s/e}$ is an average of 29 rice paddy soil- extract pairs, 13 tidal channel sediment- extract pairs, and two Sundarbans soil- extract pairs, while $D^{s/w}$ is an average of 16 rice paddy soil-water pairs. The one standard deviation error bars represent the variability across sites, season, and time of day (flood and ebb tides).

Figure 8. Average compositions of Polder 32 November samples of rice paddy soil and tidal channel sediment. No samples were collected in May. The horizontal red line represents average upper continental crust (Rudnick and Gao, 2003).

Figure 9. Comparison of average log₁₀ concentrations in tidal channel water samples from upstream (4 samples from sites B3, B8, and B9) and downstream locations (4 samples from sites P32, B2, and SB).

Preliminary Evidence of Transport-Limited Chemical Weathering and Element Immobility in the Ganges Tidal Delta Plain of Bangladesh

J. C. Ayers¹, B. Patton¹, and M. Dietrich¹

¹ Department of Earth and Environmental Sciences, Vanderbilt University. VU Station B, #351805, 2301 Vanderbilt Place, Nashville, Tennessee 37235-1805, U. S. A.

Contents of this file

Figures S1 to S8

Introduction

Figures S1-S4 are maps of sites where samples were collected. Figures S5 – S9 present additional compositional information for water, extract, soil, and sediment samples. Table S1 includes results of quantitative powder x-ray diffraction analysis of clay minerals in four tidal channel sediment samples. Table S2 lists summary statistics for measured D(solid/water) values. Table S3 lists summary statistics for measured D(solid/extract) values.

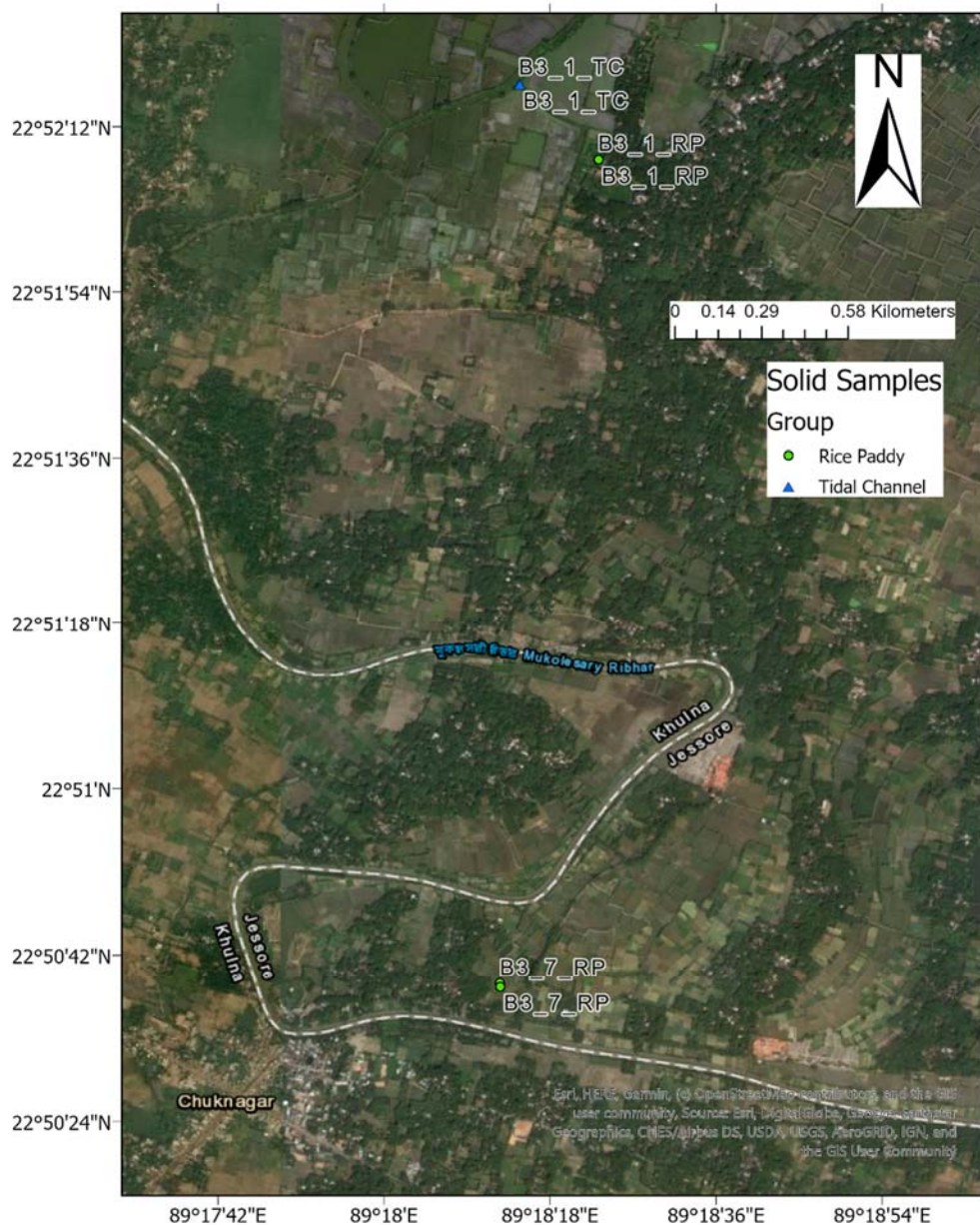


Figure S1. Map of site B3 showing locations of solid samples labeled as Site_Sample #_Sample type. Water samples were collected from the same locations. The sample types are RP rice paddy, TC tidal channel, and SB Sundarbans. GPS coordinates for each sample are in the Excel file at <https://doi.org/10.17632/6z6bdxrkbb.1>

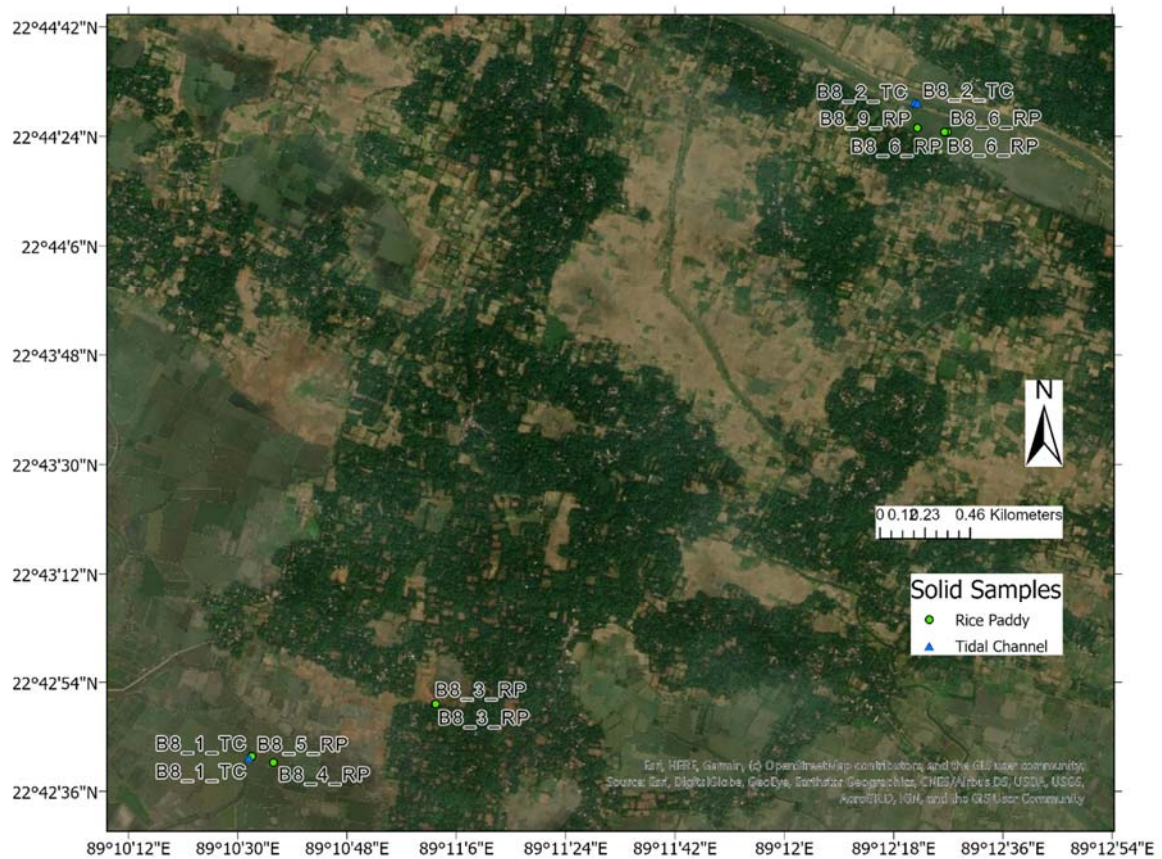


Figure S2. Map of site B8 showing locations of solid samples labeled as Site_Sample #_Sample type. Water samples were collected from the same locations. The sample types are RP rice paddy, TC tidal channel, and SB Sundarbans. GPS coordinates for each sample are in the Excel file at <https://doi.org/10.17632/6z6bdxrkbb.1>



Figure S3. Map of site B9 showing locations of solid samples labeled as Site_Sample #_Sample type. Water samples were collected from the same locations. The sample types are RP rice paddy, TC tidal channel, and SB Sundarbans. GPS coordinates for each sample are in the Excel file at <https://doi.org/10.17632/6z6bdxrkkb.1>

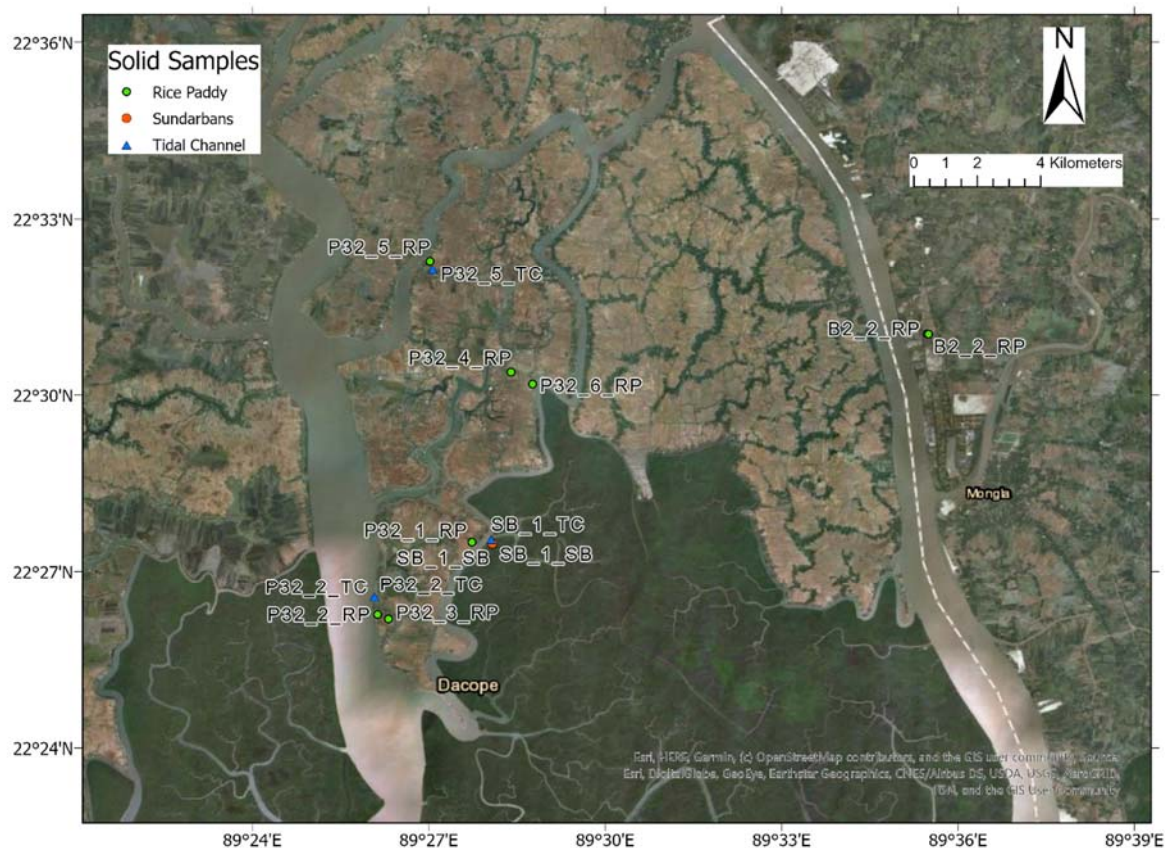


Figure S4. Map of sites B2, P32 (Polder 32), and SB (Sundarbans) showing locations of solid samples labeled as Site_Sample #_Sample type. Water samples were collected from the same locations. The sample types are RP rice paddy, TC tidal channel, and SB Sundarbans. GPS coordinates for each sample are in the Excel file at <https://doi.org/10.17632/6z6bdxrkbb.1>

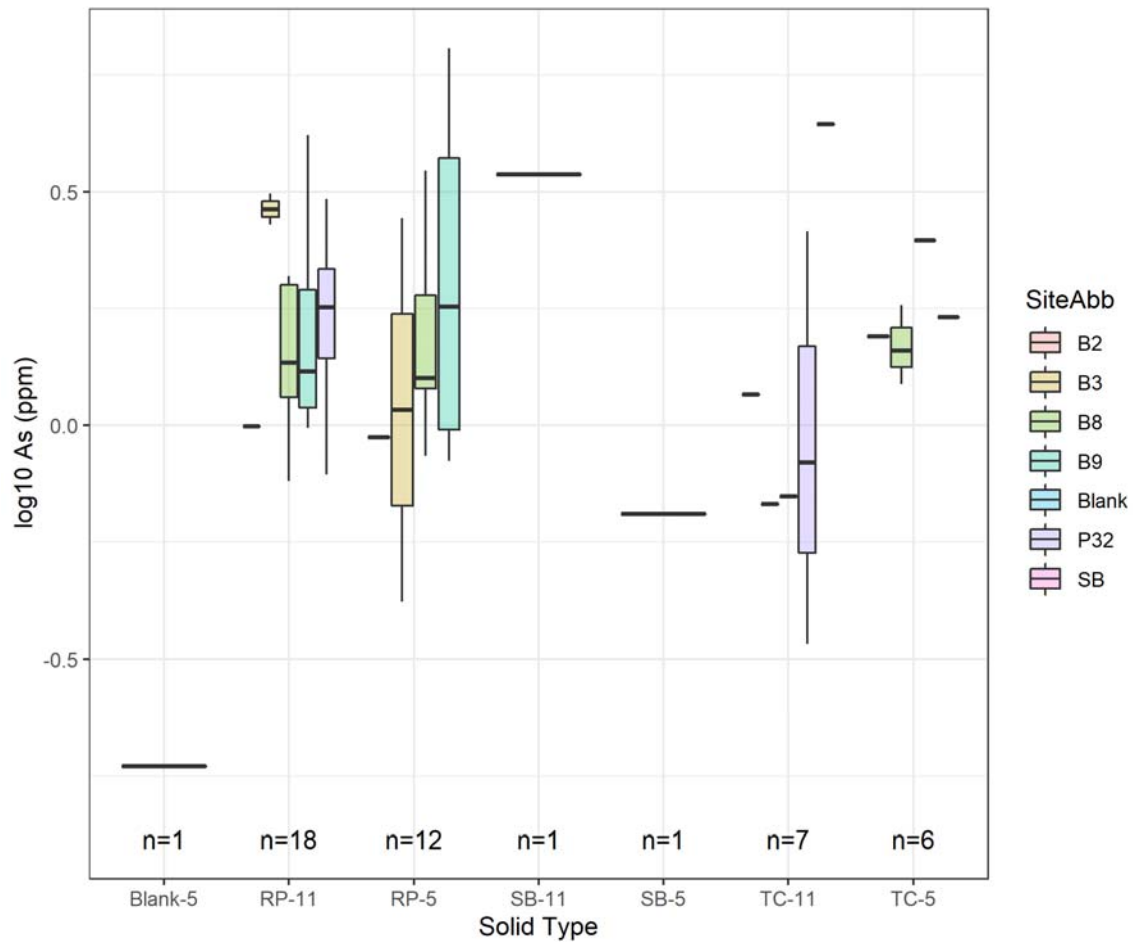


Figure S5. Boxplot of \log_{10} As concentration in ppm of solid samples classified by group (rice paddy soil RP or tidal channel sediment TC), month (dry season May=5, wet season November=11), and site. Solid types are RP = rice paddy, SB = Sundarbans, and TC = tidal channel. Sample count=n.



Fig. S6. Map showing location of tidal channel sediment samples that were analyzed for clay mineralogy using powder x-ray diffraction (results in Table S1).

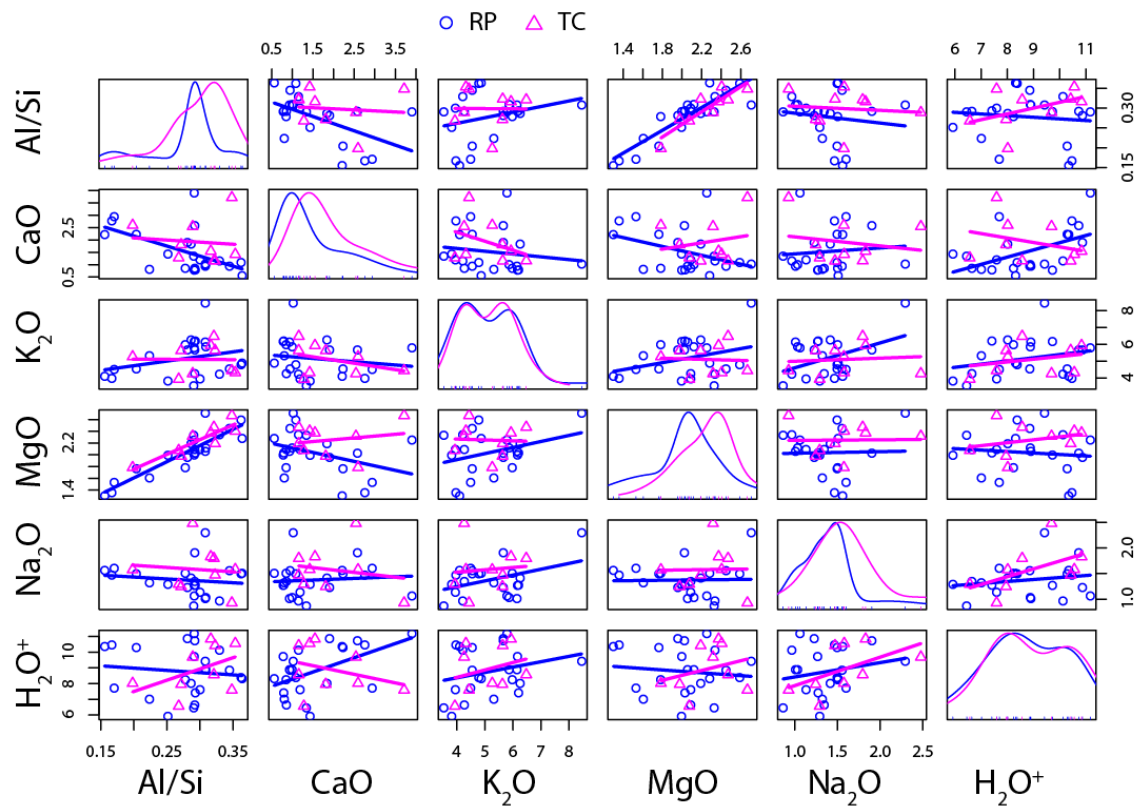


Figure S7. Scatterplot matrix of compositions of tidal channel sediment TC in pink and rice paddy soil RP compositions in blue from both wet and dry seasons. Distributions of measurements are shown in the center diagonal, and linear regressions of tidal channel sediment and rice paddy soil data are shown in each plot.

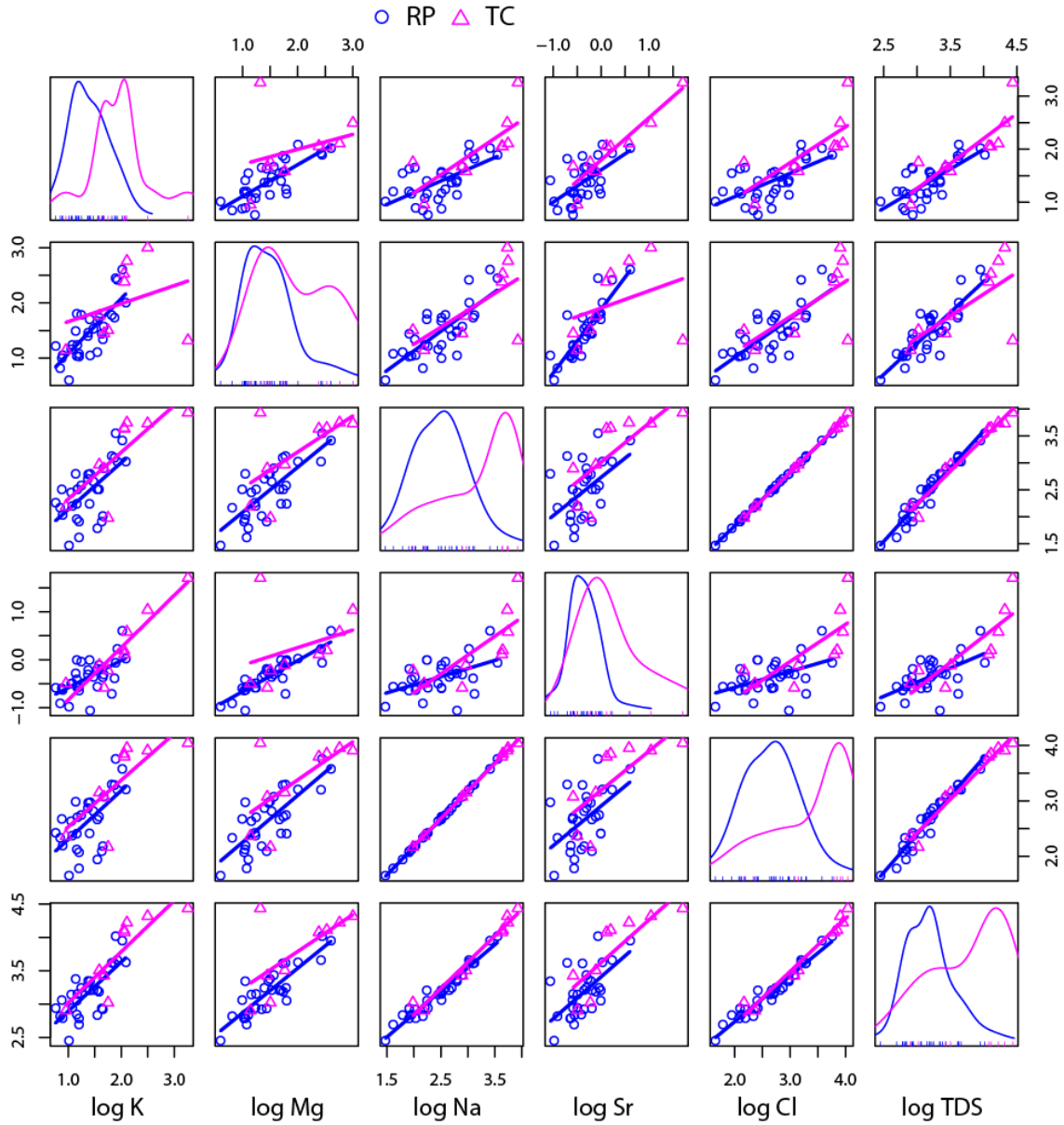


Figure S8. Scatterplot matrix of \log_{10} concentrations of conservative species in extract solutions from rice paddy soils RP in pink and tidal channel sediment samples TC in blue from both wet and dry seasons. Distributions of measurements are shown in the center diagonal, and linear regressions of tidal channel sediment and rice paddy soil data are shown in each plot.

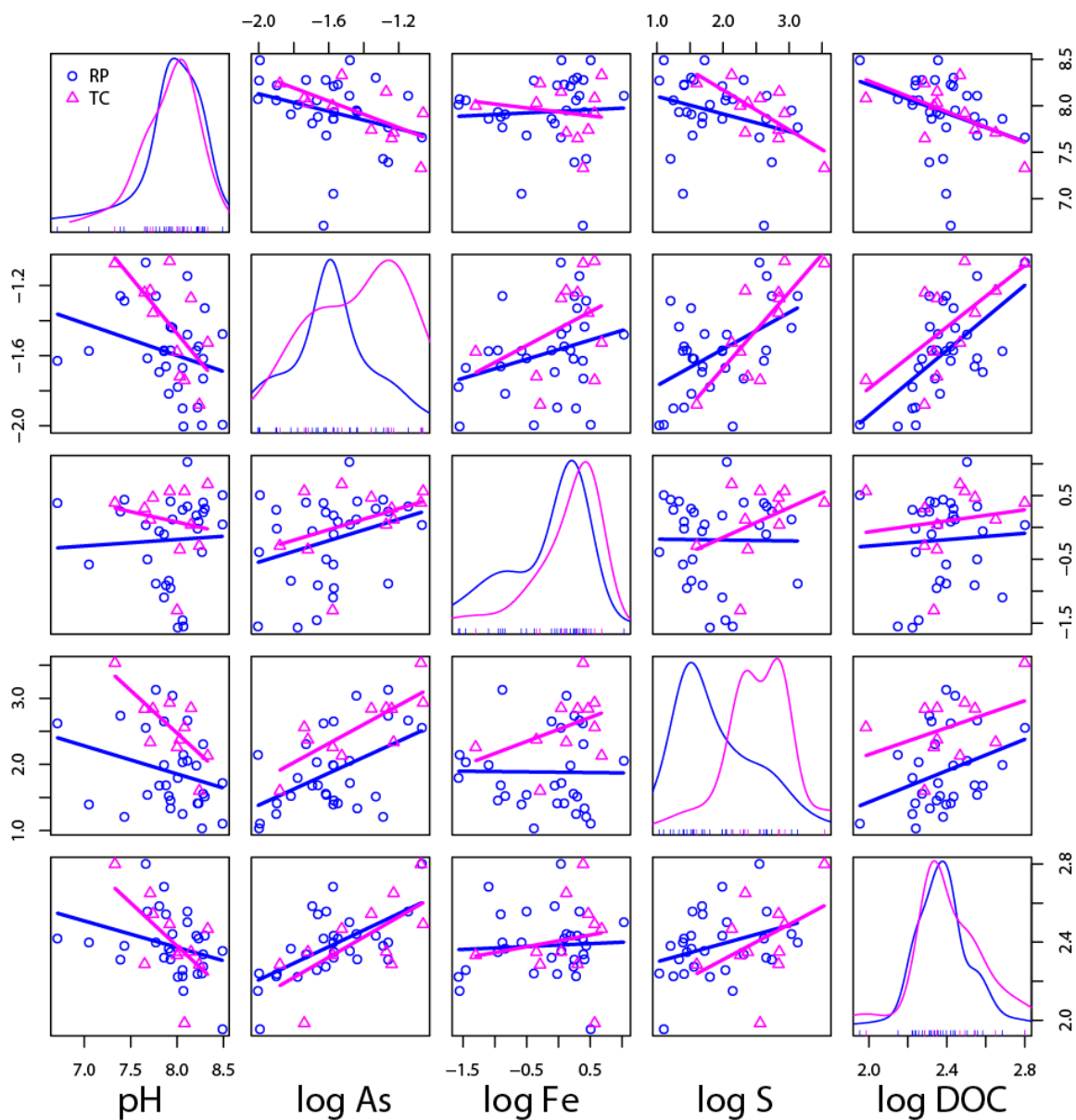


Figure S9. Scatterplot matrix of pH and \log_{10} concentrations of nonconservative species in extract solutions from rice paddy soils RP and tidal channel sediment TC samples from both wet and dry seasons. Distributions of measurements are shown in the center diagonal, and linear regressions of tidal channel sediment and rice paddy soil data are shown in each plot.

Table S1: Quantitative powder XRD clay mineralogy results

3-R-I		Peak Position	Area	Area/MIF	% Composition
	Smectite (glycol)	5.2	0	0	0.00
	Illite (air)	8.8	20.9	5.225	49.41
	Kaolinite (air)	12.3	10.7		
	Chlorite (cook)	12.3	6.25	3.12625	29.56
	Kaolinite (difference)	12.3	4.45	2.22375	21.03
				10.575	100.00
5.1-R-I		Peak Position	Area	Area/MIF	% Composition
	Smectite (glycol)	5.2	0	0	0.00
	Illite (air)	8.8	14.8	3.7	44.79
	Kaolinite (air)	12.3	9.12		
	Chlorite (cook)	12.3	0	0	0.00
	Kaolinite (difference)	12.3	9.12	4.56	55.21
				8.26	100.00
8.7-I		Peak Position	Area	Area/MIF	% Composition
	Smectite (glycol)	5.2	0	0	0.00
	Illite (air)	8.8	31.1	7.775	51.58
	Kaolinite (air)	12.3	14.6		
	Chlorite (cook)	12.3	0	0	0.00
	Kaolinite (difference)	12.3	14.6	7.3	48.42
				15.075	100.00
8.9-R-I		Peak Position	Area	Area/MIF	% Composition
	Smectite (glycol)	5.2	0	0	0.00
	Illite (air)	8.8	29.7	7.425	52.38
	Kaolinite (air)	12.3	13.5		
	Chlorite (cook)	12.3	7.54	3.7719	26.61
	Kaolinite (difference)	12.3	5.96	2.9781	21.01
				14.175	100.00

Table S2: Summary statistics for measured D(solid/water) values

	n	mean	sd	median	min	max	range	skew	kurtosis
logKdAl	12	6.29	0.15	6.26	6.06	6.53	0.46	0.22	-1.06
logKdAs	12	2.86	0.67	3.01	1.35	3.97	2.62	-0.57	0.01
logKdBa	12	2.96	0.44	2.80	2.42	3.63	1.21	0.26	-1.68
logKdCa	12	2.12	0.29	2.13	1.68	2.68	1.00	0.28	-0.86
logKdCo	12	5.46	0.54	5.66	4.35	6.18	1.83	-0.99	-0.26
logKdCr	12	4.71	0.28	4.73	4.22	5.27	1.05	0.11	-0.67
logKdCu	12	4.21	0.26	4.16	3.80	4.78	0.97	0.65	-0.23
logKdFe	11	7.35	1.04	7.44	5.36	8.62	3.26	-0.59	-0.90
logKdK	12	3.52	0.36	3.52	3.01	4.04	1.03	-0.01	-1.57
logKdMg	12	2.49	0.30	2.45	2.12	2.97	0.85	0.41	-1.33
logKdMn	12	5.23	1.36	5.80	2.68	6.46	3.78	-0.90	-0.97
logKdMo	12	3.94	0.52	3.80	3.13	4.66	1.53	0.03	-1.71
logKdNa	12	1.48	0.47	1.39	1.02	2.58	1.56	0.98	-0.15
logKdNi	12	4.88	0.48	5.05	3.88	5.68	1.79	-0.49	-0.51
logKdP	8	4.70	1.00	4.75	2.97	5.95	2.98	-0.27	-1.26
logKdS	9	1.04	0.65	0.95	0.06	2.09	2.03	0.30	-1.19
logKdSb	12	3.42	0.65	3.62	2.02	4.22	2.19	-0.71	-0.79
logKdSe	2	2.51	0.83	2.51	1.92	3.10	1.18	0.00	-2.75
logKdSi	12	4.94	0.46	5.01	3.95	5.53	1.58	-1.00	-0.13
logKdSr	12	2.33	0.23	2.33	2.01	2.67	0.67	-0.01	-1.65
logKdV	12	4.56	0.48	4.68	3.57	5.17	1.60	-0.67	-0.82
logKdZn	12	3.60	0.48	3.42	3.28	4.63	1.35	1.47	0.36

Table S3: Summary statistics for measured D(solid/extract) values

	n	mean	sd	median	trimmed	min	max	range	skew	kurtosis
logKdAl	31	5.34	0.67	5.15	5.28	4.24	7.54	3.30	1.15	1.67
logKdAs	37	2.40	0.40	2.37	2.38	1.79	3.22	1.43	0.28	-0.83
logKdBa	37	4.38	0.31	4.37	4.38	3.81	4.96	1.14	-0.09	-1.15
logKdCa	30	2.52	0.69	2.54	2.59	0.60	3.67	3.06	-0.75	0.49
logKdCo	36	4.53	0.65	4.48	4.50	3.51	6.10	2.59	0.45	-0.57
logKdCr	34	4.37	0.54	4.36	4.32	3.38	6.60	3.22	1.85	5.98
logKdCu	34	3.08	0.69	3.16	3.09	1.83	4.18	2.35	-0.25	-1.17
logKdFe	36	5.16	0.66	5.04	5.13	4.04	6.69	2.66	0.46	-0.42
logKdK	37	3.64	0.53	3.61	3.66	2.03	4.51	2.48	-0.53	0.48
logKdMg	37	3.08	0.60	3.22	3.13	1.67	3.98	2.31	-0.74	-0.33
logKdMn	37	3.90	0.87	4.04	3.97	1.97	5.07	3.10	-0.59	-0.62
logKdMo	37	2.85	0.39	2.93	2.85	1.98	3.59	1.61	-0.24	-0.34
logKdNa	36	1.86	0.68	1.86	1.87	0.46	3.28	2.82	-0.20	-0.49
logKdNi	37	3.81	0.29	3.85	3.83	3.18	4.38	1.20	-0.49	-0.35
logKdP	23	3.75	0.43	3.73	3.71	3.16	4.85	1.69	0.76	0.13
logKdS	12	0.85	0.78	1.06	0.91	-0.68	1.77	2.45	-0.57	-1.01
logKdSb	37	2.28	0.48	2.45	2.33	1.12	2.95	1.84	-0.90	-0.24
logKdSe	8	1.50	0.55	1.68	1.50	0.53	2.19	1.66	-0.49	-1.28
logKdSi	25	4.91	0.22	4.92	4.91	4.50	5.35	0.85	0.03	-0.74
logKdSr	33	2.79	0.67	2.85	2.87	0.62	3.65	3.03	-1.30	1.68
logKdV	37	4.09	0.38	4.15	4.11	3.22	4.73	1.51	-0.42	-0.79
logKdZn	29	3.74	1.02	4.04	3.71	2.23	5.62	3.39	0.04	-1.34

Table 1. Site locations and characteristics

Site	Latitude	Longitude	District	Thana	Union	Soil region ^a
B2	22.56895	89.58131	Bagerhat	Rampal	Rajnagar	Eac: Mixed Ganges River and Tidal Floodplains, non-saline
B3	22.86543	89.30501	Jessore	Keshabpur	Gaurighona	Db a or Fcb
B8	22.72527	89.19153	Satkhira	Tala	Khalishkhali	Db a: Old Southwestern Ganges River Meander Floodplains
B9	22.98833	89.48716	Jessore	Abhaynagar	Subha Para	Fcb: Old Floodplain Basins, Basin Margins
P32	22.5037	89.46009	Khulna	Dacope	Kamarkhola and Sutarkhali	Ebc: Southwestern Ganges Saline Tidal Floodplain
SB	22.4591	89.46735	Khulna	Dacope	Nalian Range	Ebd: Khulna Sundarbans Saline Tidal Floodplain

^a Soil physiographic region (Brammer, 2016).

Table 2. Element concentrations (mg/L) in water samples by sample type^a

Element	RP-11			RP-5			SB-11			TC-11			TC-5		
	count	geomean	RP-11 sd	count	geomean	RP-5 sd	count	geomean	SB-11 sd	count	geomean	TC-11 sd	count	geomean	TC-5 sd
pH	34	8.25	0.559	14	7.97	0.492	2	7.85	0.0707	8	7.7	0.214	5	7.25	0.263
SpC	34	1.02	1.51	14	5.64	9.39	2	1.63	0.686	8	1.73	1.61	5	12.5	14
Al	34	0.0297	0.00981	14	0.0534	0.0184	2	0.0298	0.00297	8	0.0315	0.0072	5	0.0546	0.0211
As	34	0.00081	0.00112	14	0.0083	0.031	2	0.00352	0.0013	8	0.00327	0.00348	5	0.00415	0.00745
B	34	0.0834	0.115	14	0.262	0.597	2	0.291	0.0176	8	0.169	0.141	5	1.15	0.981
Ba	34	0.521	1.16	14	0.175	0.124	2	1.93	0.905	8	2.21	1.86	5	0.138	0.136
Ca	34	42	16.5	14	146	144	2	43	9.41	8	51	13	5	145	85.4
Co	34	1.31E-05	1.35E-05	14	0.000438	0.000292	2	3.65E-05	8.56E-06	8	3.64E-05	3.54E-05	5	0.000333	0.000312
Cr	34	0.000491	0.000714	14	0.00146	0.000456	2	0.00171	0.000658	8	0.00143	0.00128	5	0.00202	0.000493
Cu	33	0.00143	0.00177	14	0.00453	0.00405	2	0.00215	0.00134	7	0.00237	0.000538	4	0.00908	0.0205
Fe	32	0.000787	0.00147	14	0.0257	0.0428	2	0.000346	0.000778	7	0.000712	0.000516	5	0.00356	0.00307
K	34	6.6	10.5	14	11	84.6	2	27.5	8.21	8	15.4	16.3	5	105	131
Mg	34	21.8	29.1	14	81.9	221	2	56.5	25.1	8	46.2	35.2	5	269	278
Mn	34	0.000724	0.0587	14	0.11	0.299	2	0.00126	0.000849	8	0.00115	0.000825	5	0.0421	0.12
Mo	34	0.000139	0.000143	14	0.00127	0.00139	2	0.000661	0.000163	8	0.000482	0.000536	5	0.00361	0.00229
Na	34	106	275	14	954	1900	2	494	232	8	292	343	5	2100	3030
Ni	34	0.000125	0.000203	13	0.00425	0.00416	2	0.000536	0.000104	8	0.000185	0.000386	5	0.00311	0.0027
P	20	0.00785	0.00981	14	0.194	0.416	2	0.00277	0.00622	5	0.00663	0.00628	5	0.0277	0.0104
S	34	6.94	17.7	14	21.3	239	2	40.3	19.1	8	20.6	27.5	5	167	217
Sb	34	5.26E-05	2.82E-05	14	0.000385	0.000316	2	0.000125	8.26E-05	8	0.000136	0.000151	5	0.000475	0.000133
Se	31	0.000111	0.00074	14	0.000656	0.00125	2	0.00224	0.00128	7	0.00189	0.00238	5	0.00116	0.00187
Si	34	0.965	1.06	14	4.75	6.57	2	3.15	0.0424	8	2.16	1.58	5	1.45	0.412
Sr	34	0.251	0.216	14	1	1.45	2	0.439	0.172	8	0.408	0.232	5	1.93	1.72
V	34	0.000752	0.000966	14	0.013	0.00724	2	0.00365	0.00162	8	0.00265	0.00396	5	0.0176	0.0137
Zn	34	0.0343	0.00769	13	0.0017	0.0011	2	0.0351	0.0119	8	0.0376	0.00783	5	0.00607	0.0331
Cl	34	160	438	14	1450	2960	2	756	386	8	452	543	5	3150	4510
Br	20	19.2	16.7	14	16.2	16.1	2	29.1	19.2	6	34.1	14.2	5	28.3	28
NO3	3	2.58	1.19	5	1.07	3.45				1	2.05		1	0.138	
DIC	34	31.6	9.74	14	47.1	26.8	2	34.7	16	8	29.9	7.62	5	26.3	4.46
DOC	34	33.1	8.35	10	70.6	25.3	2	34.5	15.6	8	14.4	15.7	3	37.2	9.28

^a SpC = specific conductivity in uS/cm, RP = rice paddy, TC = tidal channel, 11 = November, 5 = May, geomean = geometric mean, sd = standard deviation

Table 2. Element concentrations (mg/L) in extracts by sample type^a

	RP-11			RP-5			SB-11	SB-5	TC-11	TC-11	TC-11	TC-5	TC-5	
	count	geomean	RP-11 sd	count	geomean	RP-5 sd	(n=1)	(n=1)	count	geomean	sd	count	geomean	TC-5 sd
pH	19	7.99	0.418	12	7.83	0.323	8.46	7.93	7	8.03	0.203	5	7.76	0.32
SpC	19	435	1410	12	623	1510	280	6010	7	2040	4090	5	3940	3750
Al	17	1.83	2.31	9	0.241	0.844	5.25	9.32	7	1.38	2.19	3	2.47	2.11
As	19	0.0284	0.0203	13	0.0216	0.0118	0.0252	0.0466	7	0.0282	0.0254	5	0.0526	0.0206
B	4	0.488	0.508	3	0.109	0.108			2	1.99	12			
Ba	19	0.133	0.0937	13	0.133	0.0409	0.062	0.231	7	0.158	0.165	5	0.318	0.255
Ca	17	71.6	119	12	145	64.6	28		5	224	2480	2	637	1180
Co	19	0.0016	0.0031	10	0.000764	0.0013	0.000497	0.00303	7	0.00185	0.00218	5	0.00309	0.00507
Cr	17	0.0131	0.0226	13	0.00474	0.00484	0.00935	0.0152	7	0.0104	0.00805	4	0.0176	0.00351
Cu	15	0.0537	0.061	12	0.0534	0.0579	0.085	0.211	7	0.219	0.587	5	0.283	0.483
Fe	19			13	0.205	0.784	4.68	4.99	6	1.88	1.79	5	0.812	0.914
K	19	24.9	36	13	25.6	18.7	29.1	106	7	72.2	664	5	110	104
Mg	19	27.6	102	13	34.9	70.2	17.7	134	7	48.8	204	5	166	397
Mn	19	0.108	0.435	13	0.0993	0.379	0.046	2.49	7	0.675	7.25	5	2.73	6.63
Mo	19	0.0127	0.0156	13	0.00943	0.00553	0.0173	0.0209	7	0.0184	0.00966	5	0.0202	0.0135
Na	19	313	656	13	307	915	282	3770	7	1210	3200	5	1500	2380
Ni	19	0.017	0.0134	13	0.0177	0.013	0.0137	0.018	7	0.0186	0.00777	5	0.0303	0.0238
P	14	0.265	0.277	11	0.266	0.268			3	0.843	0.792	2	0.472	0.759
S	19	98.8	374	13	54.5	141	104	391	7	224	314	5	581	1350
Sb	19	0.00686	0.00669	13	0.00514	0.00443	0.00595	0.00321	7	0.0058	0.00415	5	0.00518	0.00288
Se	19	0.0175	0.0125	12	0.0123	0.0182	0.01	0.0493	7	0.0195	0.023	5	0.0533	0.0794
Si	15	11.9	6.78	12	14.5	5.41	19.4		4	14.7	12.1	1	24.3	
Sr	18	0.366	0.936	13	0.556	0.246	0.147		5	1.65	22.2	4	1.91	4.92
V	19	0.026	0.0159	13	0.0186	0.0182	0.0221	0.0649	7	0.0256	0.0279	5	0.0466	0.026
Zn	13	0.0331	0.0808	11	0.0106	0.147	0.0105	0.76	5	0.41	0.58	4	0.794	0.199
Cl	19	469	970	13	462	1490	425	5810	7	1800	4390	5	2290	3590
Br	9	26.4	16.7	3	38.3	137		22.6	5	17.9	15.1	4	28.2	29.1
NO3	6	8.26	12.6	8	29.5	42		2.78	2	2.07	0.0348	5	3.03	4.03
DIC	19	43	28.1	13	53.8	22.3	61.7	51.9	7	51	20	5	47.5	11.3
DOC	19	244	113	13	229	97.3	206	196	7	213	91.7	5	305	191

^a SpC in uS/cm, RP = rice paddy, TC = tidal channel, 11 = November, 5 = May, geomean = geometric mean, sd = standard deviation

Table 4. Concentrations in solid samples by sample type in ppm^a

Element	RP-11			RP-5			SB-11		SB-5		TC-11		TC-5	
	count	geomean	RP-11 sd	count	geomean	RP-5 sd	(n=1)	(n=1)	count	geomean	TC-11 sd	count	geomean	TC-5 sd
Al	18	63800	12700	12	57000	14200	77800	32500	7	57100	15500	6	59000	10200
As	18	1.63	0.939	12	1.53	1.71	3.45	0.645	7	1.09	1.46	6	1.66	0.431
B	18	828000	137000	12	791000	160000	1060000	874000	7	889000	99700	6	819000	134000
Ba	18	768	296	12	917	244	492	378	7	638	331	6	728	333
Ca	18	7600	4980	12	11200	9070	12300	9580	7	13400	4600	6	10000	3670
Co	18	11	9.49	12	8.19	3.44	12.2	8.45	7	8.56	3.27	6	8.95	1.94
Cr	18	55.3	11.3	12	47.9	17.8	94.1	18.2	7	39.7	22.6	6	51.5	10.8
Cu	18	29.4	7.16	12	27.5	16.8	37.5	23.4	7	27.3	8.35	6	28.3	9.78
Fe	18	30500	8000	12	27200	11700	47600	10900	7	25100	12200	6	28900	5510
K	18	36300	5340	12	36100	7660	33400	26700	7	33700	7990	6	34800	8540
Mg	18	10700	2090	12	10000	2580	13100	10500	7	11300	1450	6	10600	1640
Mn	18	432	169	12	408	143	693	417	7	592	144	6	455	40.1
Mo	18	1.96	2.22	12	1.8	1.59	12.5	0.945	7	1.84	1.27	6	1.28	0.785
Na	18	7990	1890	12	8090	1660	10700	11800	7	9530	2120	6	9850	1640
Ni	18	27.8	6.71	12	26.6	13.1	32.1	20.6	7	23.3	9.31	6	24.3	6.18
P	18	367	177	12	416	181	802	98.4	7	276	218	6	422	51.4
S	12	101	86.1	7	72.5	115	535	311	6	71.8	277	5	79.6	211
Sb	18	0.249	0.206	12	0.356	0.352	0.379	0.0246	7	0.109	0.173	6	0.275	0.193
Se	5	0.0912	0.157	2	0.209	0.315			1	0.286		3	0.205	0.35
Si	18	227000	49400	12	224000	39400	330000	73700	7	167000	85500	6	209000	21700
Sr	18	82.9	15	12	84.3	14.3	121	88.7	7	95.8	13.7	6	82.4	13.2
V	18	73.1	26	12	78	25.2	103	21.6	7	40.5	39.7	6	72.7	15.6
Zn	18	77.8	13.5	12	72.2	19.4	83.4	53.7	7	70	13.2	6	73.5	10.3
H ₂ O ⁺	16	73700	13100	10	78600	17900	60000	61000	5	68600	14900	5	73600	10200
H ₂ O ⁻	16	23400	9020	10	25200	17800	22000	38000	5	19100	11800	5	29000	20100

^a RP = rice paddy, TC = tidal channel, 11 = November, 5 = May, geomean = geometric mean, sd = standard deviation

Table 5: Measured grain sizes of select samples^a

Sample Name	Median (μm)	Mode (μm)	Volume- Weighted Mean (μm)
BEMS_09_TC_01_Nov	16.37	14.98	28.44
BEMS_08_RP_06M_May	36.29	53.68	46.55
SB_SB_1_May	36.02	57.87	47.97
BEMS_03_RP_07_Nov	21.41	23.15	43.16
BEMS_08_TC_01_May	9.89	6.72	20.55
BEMS_08_RP_06M_Nov	39.67	52.41	60.23
BEMS_08_TC_02_May	22.95	34.62	30.33
BEMS_03_TC_01_May	8.44	6.45	14.52

^a Sample Name given as Site_Sample type_Sample # _Month,
TC = tidal channel, RP = rice paddy, SB = Sundarbans

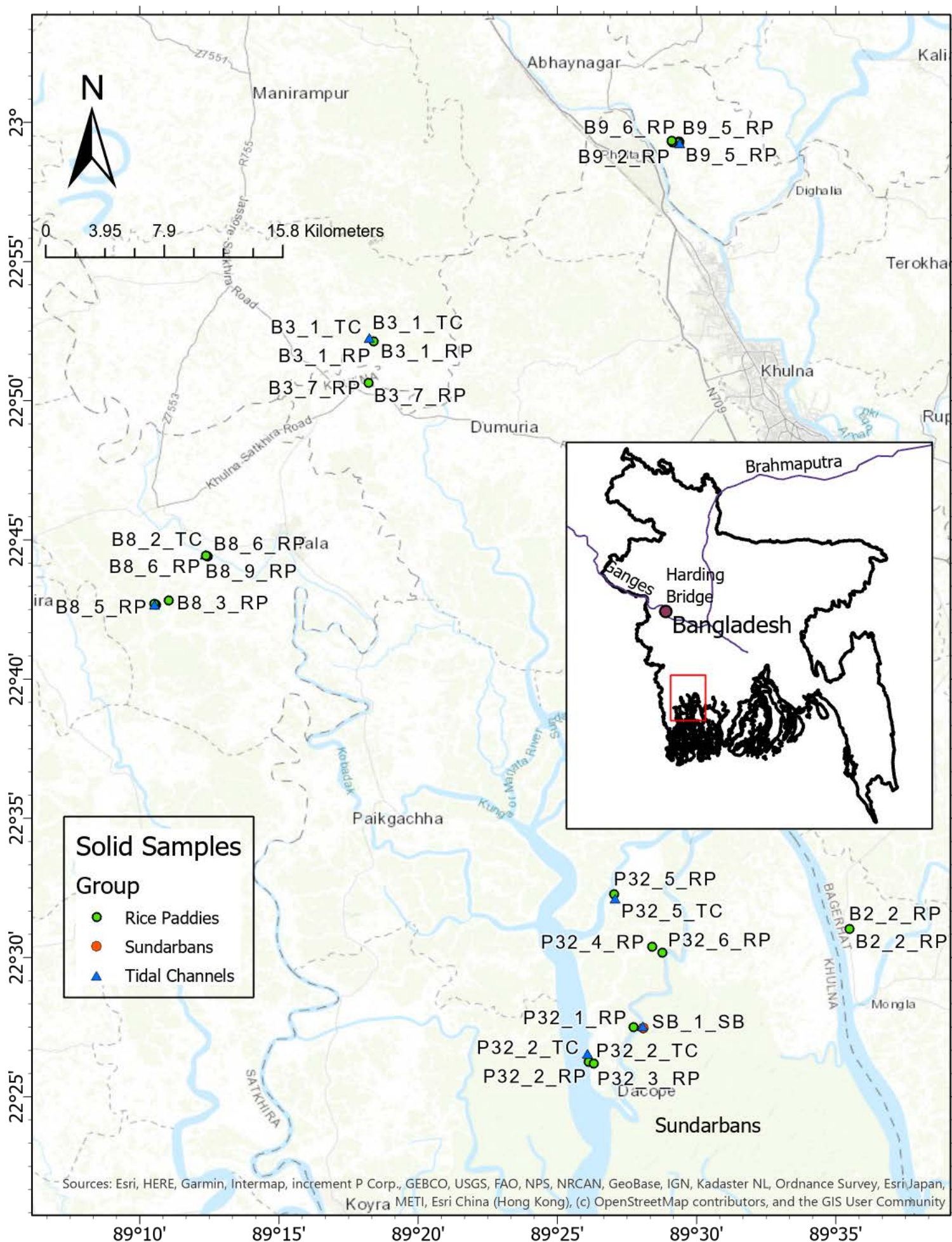
Table 6: Concentrations of oxides in solid samples^a

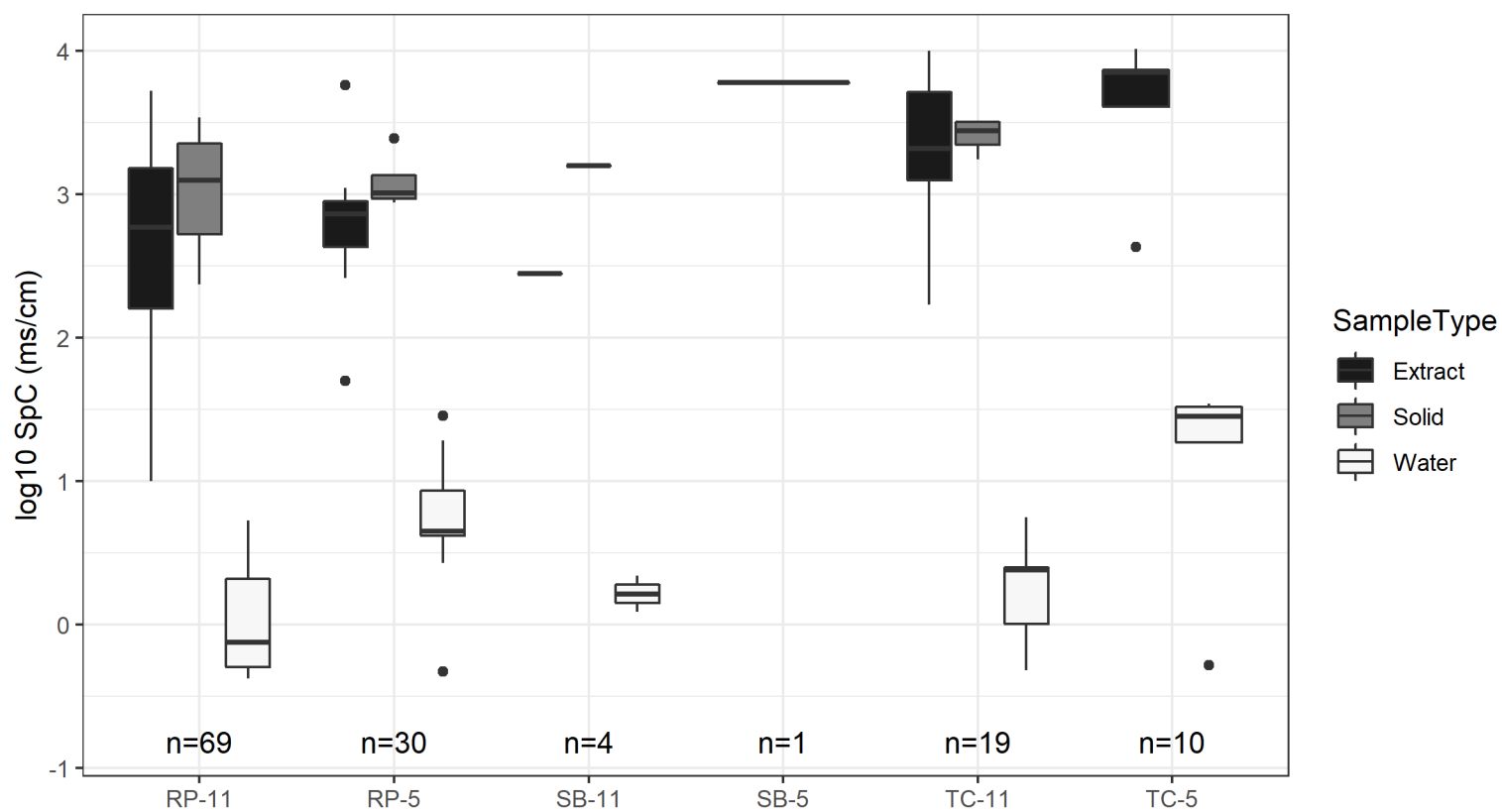
Oxide	RP mean ^b	St Dev	TC mean	St Dev	Avg. UCC ^c	RP anhydrous mean	StDev	TC anhydrous mean	StDev
SiO ₂	59.4	3.75	57.2	4.46	67.1	67.2	3.84	65.3	3.2
Al ₂ O ₃	14	2.37	14.3	1.61	15.5	15.8	2.64	16.4	2.01
FeO	1.35	0.317	1.58	0.44	5.07	1.54	0.36	1.81	0.514
MgO	5.07	1.14	5.1	0.888	2.5	5.76	1.3	5.85	1.13
CaO	4.62	1.11	5.01	0.732	3.61	5.23	1.24	5.73	0.862
Na ₂ O	2.04	0.36	2.25	0.272	3.29	2.31	0.406	2.58	0.341
K ₂ O	1.46	0.87	1.91	0.869	2.82	1.66	1.02	2.17	0.938
P ₂ O ₅	0.117	0.0368	0.121	0.0314	0.15	0.133	0.0409	0.139	0.036
H ₂ O ⁺	8.78	1.53	8.91	1.52					
H ₂ O ⁻	3.01	1.35	3.59	2.1					
Sum	100		100			100		100	

^a Four samples with anomalously low SiO₂ were not included in these summary statistics.
Concentrations of oxides normalized to 100%.

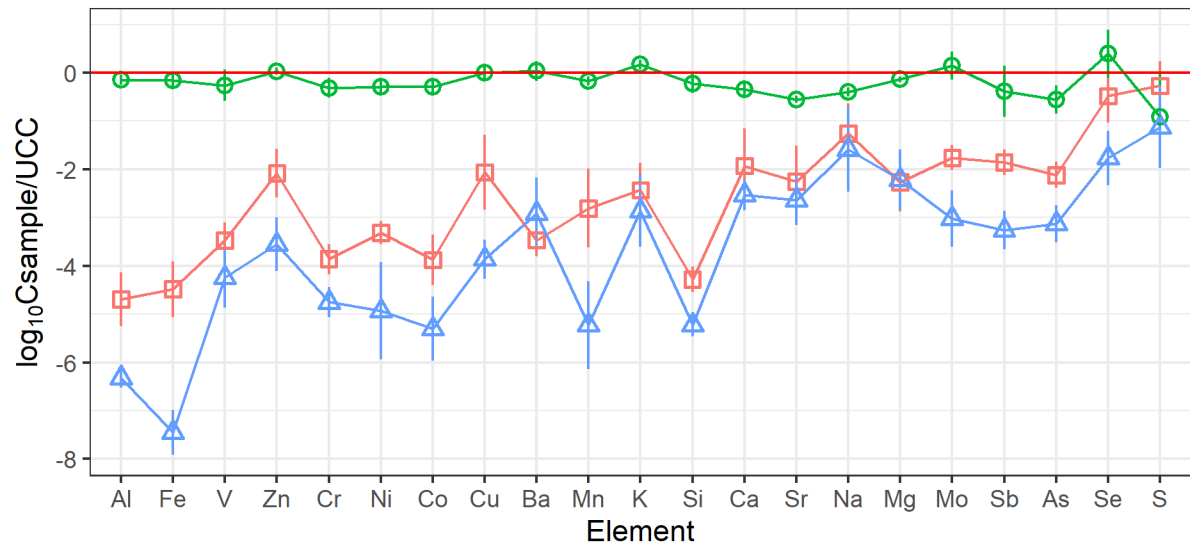
^b Mean values are 5% trimmed mean, RP = rice paddy soil, TC = tidal channel sediment




^c Rudnick and Gao (2003)

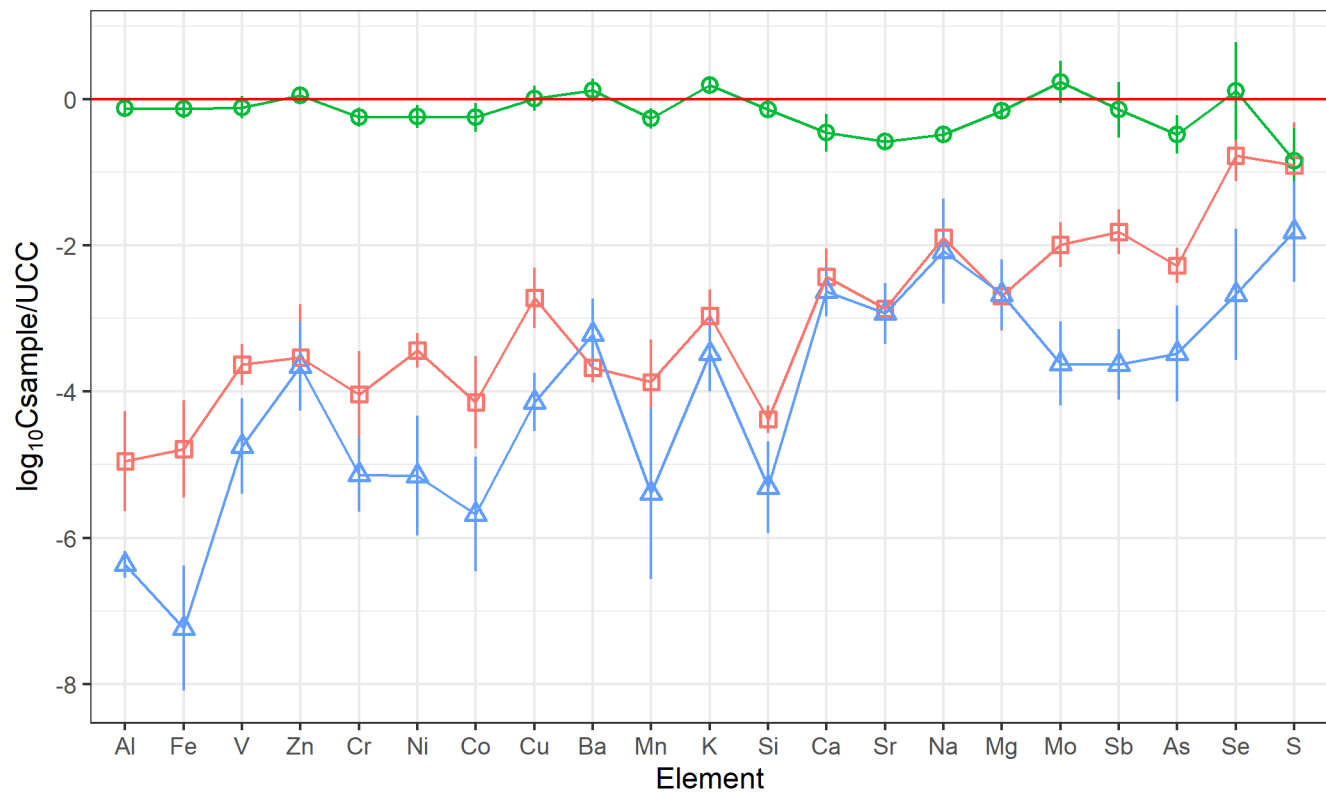




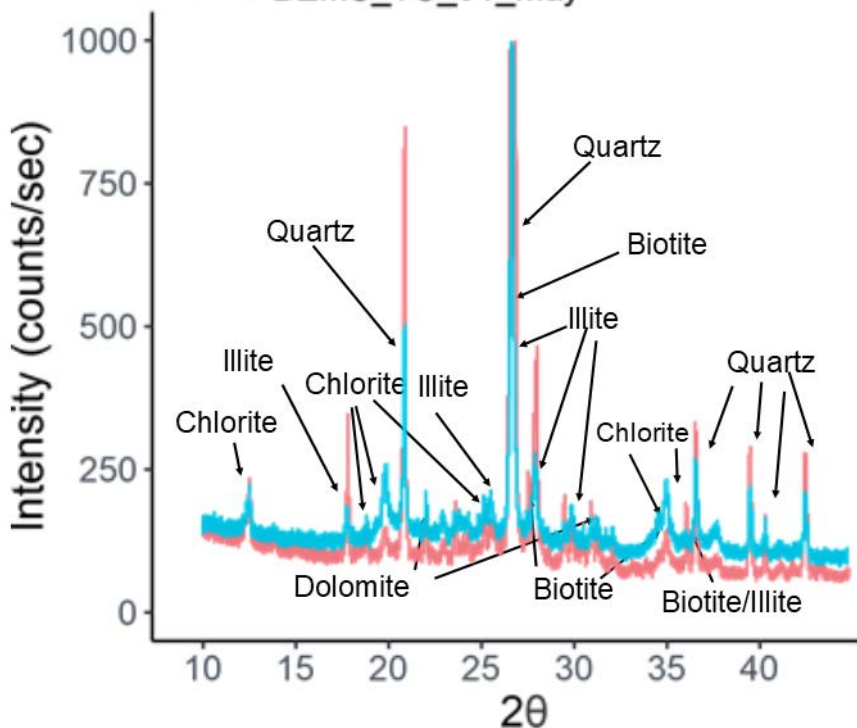
SampleType ■ Extract ⊕ Solid ▲ Water

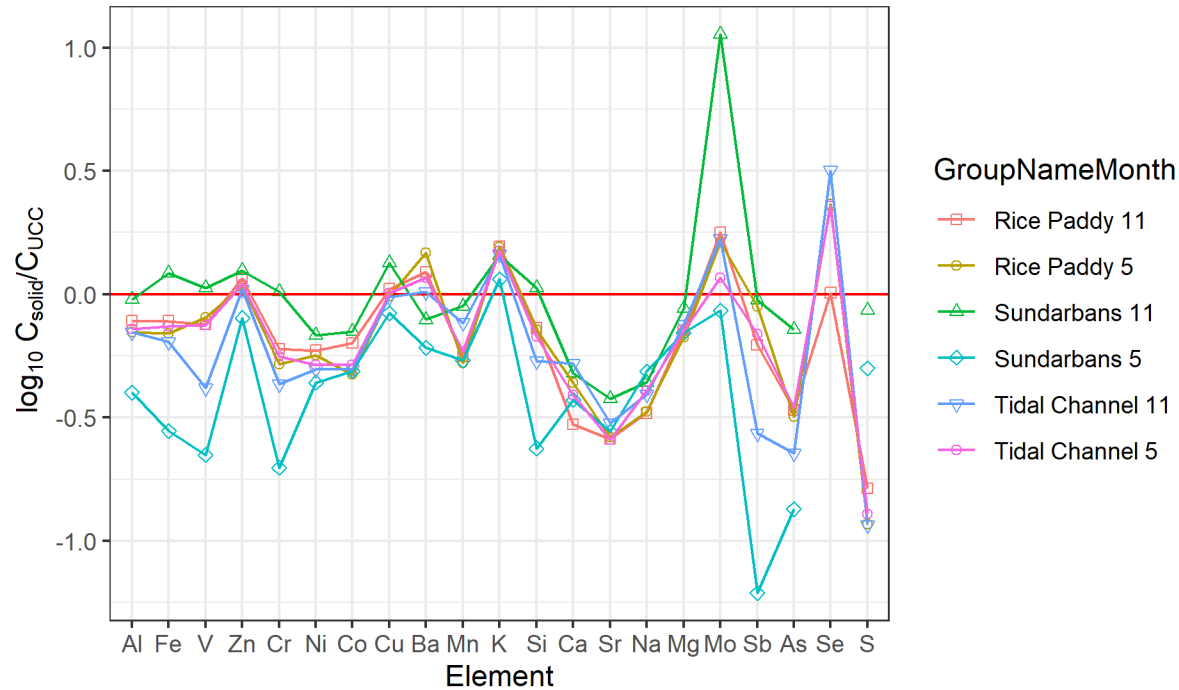


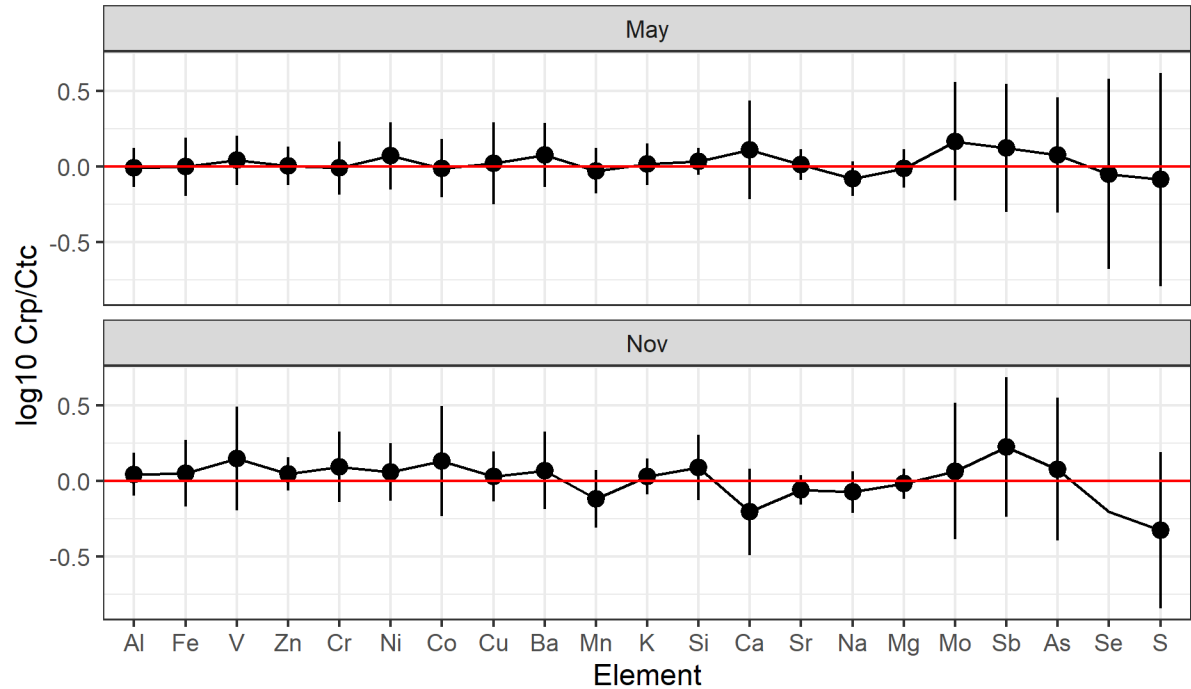
SampleType  Extract  Solid  Water



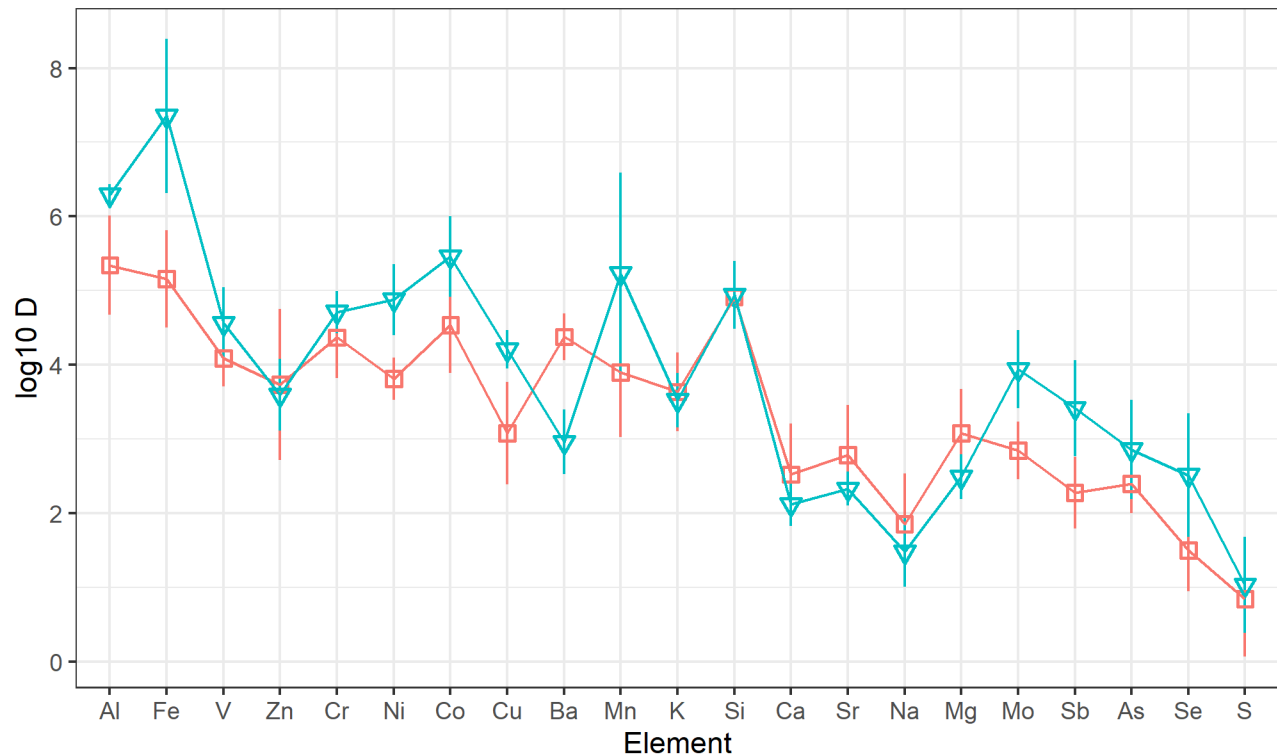
Sample — BEMS_08_RPS_06M_May
— BEMS_TC_01_May

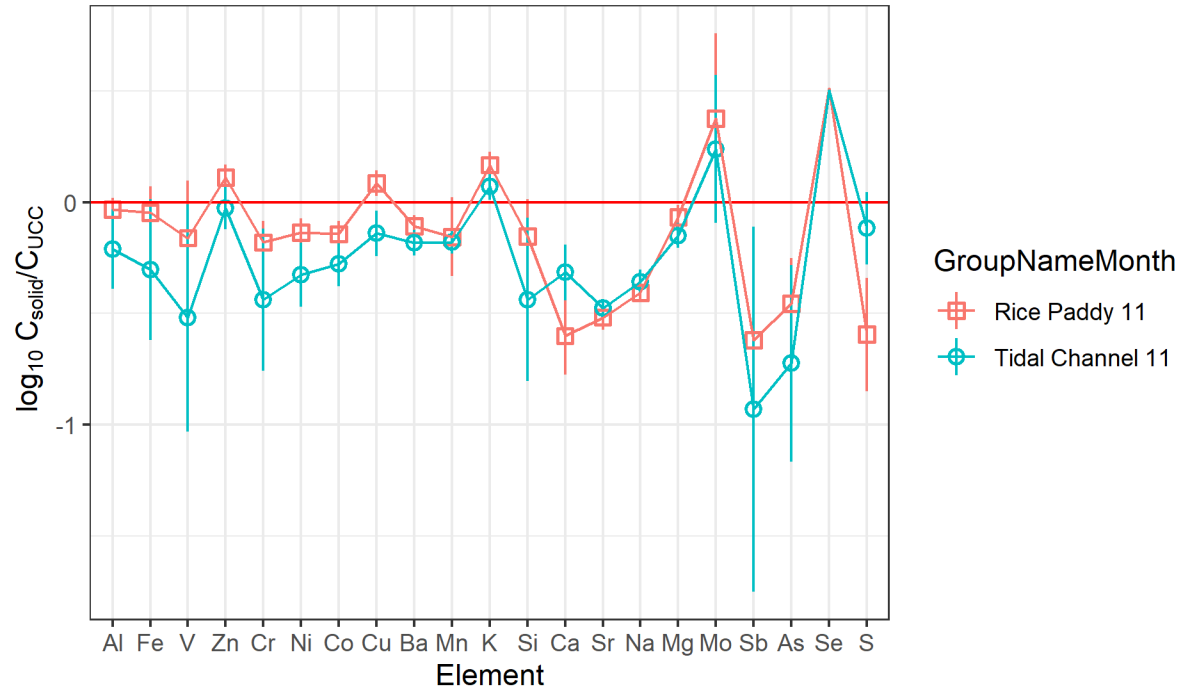








Dtype ■ Solid/Extract ▼ Solid/Water





Location  Downstream  Upstream

